

# VLT/ISAAC Spectra of the $H\beta$ Region in Intermediate-Redshift Quasars

## II. Black Hole Mass and Eddington Ratio\*

J. W. Sulentic<sup>1</sup>, P. Repetto<sup>2,3</sup>, G. M. Stirpe<sup>4</sup>, P. Marziani<sup>2</sup>, D. Dultzin-Hacyan<sup>3</sup>, and M. Calvani<sup>2</sup>

<sup>1</sup> Department of Physics and Astronomy, University of Alabama, Tuscaloosa, AL 35487, USA  
e-mail: [giacomo@merlot.astr.ua.edu](mailto:giacomo@merlot.astr.ua.edu)

<sup>2</sup> Osservatorio Astronomico di Padova, INAF, Vicolo dell' Osservatorio 5, 35122 Padova, Italy  
e-mail: [marziani@pd.astro.it](mailto:marziani@pd.astro.it); [calvani@pd.astro.it](mailto:calvani@pd.astro.it)

<sup>3</sup> Instituto de Astronomía, UNAM, Aptdo. Postal 70-264, México, D. F. 04510, México e-mail:  
[prepetto@astrocu.unam.mx](mailto:prepetto@astrocu.unam.mx), [deborah@astrocu.unam.mx](mailto:deborah@astrocu.unam.mx)

<sup>4</sup> Osservatorio Astronomico di Bologna, INAF, Via Ranzani 1, 40127 Bologna, Italy  
e-mail: [stirpe@bo.astro.it](mailto:stirpe@bo.astro.it)

Received / Accepted

**Abstract.** We derive black hole masses for a sample of about 300 AGNs in the redshift range  $0 < z < 2.5$ . We use the same virial velocity measure (FWHM  $H\beta_{BC}$ ) for all sources which represents a significant improvement over previous studies. We review methods and caveats for determining AGN black hole masses via the virial assumption for motions in the gas producing low ionization broad emission lines. We derive a corrected FWHM( $H\beta_{BC}$ ) measure for the broad component of  $H\beta$  that better estimates the virialized line emitting component by comparing our FWHM measures with a sample of reverberated sources with  $H\beta$  radial velocity dispersion measures. We also consider the FWHM of the FeII $\lambda$ 4570 blend as a potential alternative velocity estimator. We find a range of black hole mass between  $\log M_{BH} \sim 6.0$ – $10.0$ , where  $M_{BH}$  is in solar masses. Estimates using corrected FWHM( $H\beta$ ), as well as FWHM(FeII) measures, reduce the number of sources with  $\log M_{BH} > 9.5$  and suggest that extremely large  $M_{BH}$  values ( $\log M_{BH} \gtrsim 10$ ) may not be realistic. Derived  $L/L_{Edd}$  values show no evidence for a significant population of super-Eddington radiators especially after correction is made for sources with extreme orientation to our line of sight. Sources with FWHM( $H\beta_{BC}$ )  $\lesssim 4000$  km s<sup>-1</sup> show systematically higher  $L/L_{Edd}$  and lower  $M_{BH}$  values than broader lined AGNs (including almost all radio-loud sources).

**Key words.** quasars: emission lines – quasars: general – line: profiles – black hole physics

### 1. Introduction

Gravitational accretion onto supermassive black holes is generally accepted as the ultimate energy source of Active Galactic Nuclei (AGNs). The last decade has seen a major effort to derive reasonable estimates of black hole masses ( $M_{BH}$ ) by assuming virialized motions in the broad line emitting gas:

$$M_{BH} = \frac{v^2 r_{BLR}}{G} \quad (1)$$

where  $v$  is the velocity dispersion of the emitting gas at distance  $r_{BLR}$ . The velocity dispersion can be written as  $v = f \text{FWHM}$  where FWHM is

the full width half maximum measured for a suitable emission line. The factor  $f$  depends on the geometry and details of the kinematics (Krolik, 2001; McLure & Dunlop, 2001; Onken et al., 2004). The usefulness of the virial assumption for  $M_{BH}$  determination is best exploited using reverberation-mapping studies, especially for the Balmer lines (Koratkar & Gaskell, 1991; Peterson & Wandel, 1999; Wandel et al., 1999; Kaspi et al., 2000; Peterson et al., 2004). Kaspi et al. (2000, 2005) derive a relation between Broad Line Region (BLR) distance  $r_{BLR}$  and continuum luminosity

$$r_{BLR} \propto (\lambda L_\lambda)^\alpha \quad (2)$$

where the exponent  $\alpha$  is constrained between 0.5 and 1.0, and is most likely  $\approx 0.6$ – $0.7$  for broad  $H\beta$  ( $H\beta_{BC}$ ) and optical continuum luminosity.

Send offprint requests to: J. W. Sulentic

\* Based on observations collected at the European Southern Observatory, Chile. Proposal ref.: ESO 072.B-0338(A)

There are caveats associated with this method. The virial assumption is not likely to be generally valid for the emission line gas in AGNs. It has been known for several decades that different emission lines in a source can show different width and profile shape (e.g., de Robertis, 1985; Sulentic, 1989). The virial assumption implies that the velocity dispersion will steadily decrease with distance from the central black hole  $\propto r^{-\frac{1}{2}}$ . The time lag between continuum fluctuations and corresponding emission line responses will therefore anti-correlate with line width. This trend has been confirmed in a few objects (Peterson & Wandel, 2000).

Observations however show that profile width and shape depend on the ionization potential. The strongest high-ionization lines (HILs; e.g.  $\text{CIV}\lambda 1549$ ) often display blueward asymmetric profiles, or even centroid blueshifts (up to several  $1000 \text{ km s}^{-1}$ ) with respect to the best estimates of the rest frame of the source (e.g., Gaskell, 1982; Marziani et al., 1996; Richards et al., 2002; Bachev et al., 2004). Blueshifts like those observed for  $\text{CIV}\lambda 1549$  are indicative of obscuration and radial motions which invalidate the virial assumption.

Low ionization lines (LILs) like  $H\beta$  are the best candidates for emission arising from a virialized medium. All or much of the Balmer (and  $\text{FeII}$ ) line emission is thought to arise from an accretion disk or a flattened cloud distribution near the disk (e.g., Collin-Souffrin et al., 1988; Marziani et al., 1996). A major caveat, especially for the Balmer lines, involves the possibility that: (1) there are two or more emission components in a line, and (2) only one of them may arise in a region where the virial assumption holds. The Balmer lines do not usually show very large line shifts (i.e., shift  $\leq$  FWHM) although profiles can be very asymmetric. Both red and blue asymmetries are observed for  $H\beta_{\text{BC}}$  which is the most studied line because it is relatively unblended and is observable with optical spectrometers up to  $z \approx 1$  (Osterbrock & Shuder, 1982; Sulentic, 1989; Stirpe, 1990; Sulentic et al., 1990; Corbin, 1991; Corbin & Francis, 1994).

The most ambiguous sources from the point of view of  $M_{\text{BH}}$  determination show  $\text{FWHM}(H\beta_{\text{BC}}) \gtrsim 4000 \text{ km s}^{-1}$  (Population B, following Sulentic et al., 2000b) and redshifted profiles and/or red asymmetries. Not all parts of the  $H\beta$  profile respond to continuum changes in the same way implying that some of the line emitting gas may be optically thin or, less likely, is not exposed to the variable HI ionizing radiation (we will return to this issue in §5.2). The broad line profile in Pop. B sources may be due to two distinct emitting regions: (1) an optically thick classical BLR and (2) a broader and redshifted very broad component that may be optically thin or marginally optically thick to the Lyman continuum, originating in a distinct Very Broad Line Region (VBLR) (Marziani & Sulentic, 1993; Shields et al., 1995; Sulentic et al., 2000c). The redshift of the VBLR component raises doubts that it arises from virialized gas. A strong BLR response to continuum fluctuations, coupled with a weak or absent response of the VBLR component, can lead to an overestimate of FWHM

for the virialized BLR component resulting in an overestimate of  $M_{\text{BH}}$  (Wandel et al., 1999; Kaspi et al., 2000; Vestergaard, 2002).

Sources with  $\text{FWHM}(H\beta_{\text{BC}}) \lesssim 4000 \text{ km s}^{-1}$  (Population A, Sulentic et al., 2000b) should provide more reliable  $M_{\text{BH}}$  estimates. The  $H\beta_{\text{BC}}$  profile is usually well fit with a symmetric function (Véron-Cetty et al., 2001; Sulentic et al., 2002) and the BLR emission is thought to arise from a Keplerian disk. The most unreliable Pop. A sources, in a disk emission scenario, should be those observed near face-on where the rotational (i.e. virial) contribution to  $\text{FWHM}(H\beta_{\text{BC}})$  is minimal. At least some of the face-on sources may be identified as the so-called “blue outliers” which show a weak and significantly blueshifted  $[\text{OIII}]\lambda\lambda 4959, 5007$  lines (Zamanov et al., 2002; Marziani et al., 2003b; Aoki et al., 2005; Boroson, 2005). The inferences in this, and the preceding paragraph have emerged from the Eigenvector 1 (E1) scenario that we have pursued for the past 5+ years (Sulentic et al., 2000a,b, following Boroson & Green (1992)). The results reported in this paper appear to confirm them.

There are additional caveats connected with using  $\text{FWHM}(H\beta_{\text{BC}})$  for  $M_{\text{BH}}$  derivations. Line asymmetries can affect  $M_{\text{BH}}$  estimates for both Pop. A and B sources. The  $v_r$  displacement of the line centroid at fractional intensities (at half maximum,  $c(\frac{1}{2})$ ) can give useful information about the uncertainty of  $\text{FWHM}(H\beta_{\text{BC}})$  measurements. The average displacement value is a few hundred  $\text{km s}^{-1}$  with median  $c(\frac{1}{2}) \approx 400 \text{ km s}^{-1}$  (Marziani et al., 2003a). This implies that deviations from a symmetric profile can affect  $M_{\text{BH}}$  estimates by  $\approx 40 \%$ . Uncertainties are also introduced by: (1) contamination from overlapping/nearby lines such as  $\text{FeII}$ ,  $\text{HeII}\lambda 4686$ , and  $[\text{OIII}]\lambda\lambda 4959, 5007$  (Osterbrock & Shuder, 1982; de Robertis, 1985; Joly, 1988; Jackson et al., 1991), (2) FWHM measures based on single-epoch observations, (3) low  $S/N$  spectra and (4) spectra without  $H\beta$  narrow component ( $H\beta_{\text{NC}}$ ) subtraction. The  $r_{\text{BLR}} - L_{\lambda}$  relation is also not free from uncertainties. Reverberation mapping-based  $M_{\text{BH}}$  determinations are certainly affected by the non-negligible radial extent of the optically thick BLR. The derived  $r_{\text{BLR}}$  is not a very well defined quantity and  $\alpha$  is also somewhat uncertain because of the intrinsic scatter in the correlation. Finally, reverberation data does not exist for high luminosity/redshift quasars requiring an extrapolation of the  $r_{\text{BLR}} - L_{\lambda}$  relation in order to estimate  $M_{\text{BH}}$  for these sources.

Uncertainties for  $M_{\text{BH}}$  derivations using single profile observation of  $H\beta_{\text{BC}}$  are estimated to be a factor of 2–3 (at a 1  $\sigma$  confidence level), but may be as low as 30% if the velocity dispersion of the variable part of  $H\beta_{\text{BC}}$  profile is employed as a virial estimator (Peterson et al., 2004).  $M_{\text{BH}}$  estimates based on the virial relation retain a statistical validity considering that AGNs span a 5dex range in  $M_{\text{BH}}$  ( $10^5 M_{\odot} \lesssim M_{\text{BH}} \lesssim 10^{10} M_{\odot}$ ) and that the relation has now been applied to large samples of objects ( $\sim 10^3$ ; McLure & Dunlop, 2004).

With these considerations in mind, and supported by previous results, we use the virial relation to compute  $M_{\text{BH}}$  for  $\approx 280$  AGNs in our E1 sample of low redshift ( $0 \lesssim z \lesssim 1$ ) sources (Marziani et al., 2003b) supplemented with 25 intermediate redshift/high luminosity ( $1 \lesssim z \lesssim 2.5$ ) quasars. We derive  $M_{\text{BH}}$  and  $L/L_{\text{Edd}}$  values in several ways. New VLT-ISAAC data are presented for 9 sources (§2) which supplement data already published for sixteen quasars (Sulentic et al., 2004). Line measures are presented in §4. We use H $\beta_{\text{BC}}$  and FeII $\lambda$ 4570 line widths in a consistent way over the redshift range  $0 \lesssim z \lesssim 2.5$  (a range of  $10^5$  in luminosity). We compute black hole mass  $M_{\text{BH}}$ , Eddington ratio  $L/L_{\text{Edd}}$  (§5) and we discuss how mass determinations might be improved (§5.2) so that the evolution of  $M_{\text{BH}}$  and  $L/L_{\text{Edd}}$  with redshift can be considered (§5.3 and §6).

## 2. Observations and Data Reduction

New intermediate redshift data were obtained between 10/2003-03/2004 in service mode with the infrared spectrometer ISAAC mounted on VLT1 (ANTU) at the European Southern Observatory. Each spectrum corresponds to a wavelength range (IR windows sZ, J, sH) that covers the region of redshifted H $\beta_{\text{BC}}$  and FeII $\lambda$ 4570 or FeII $\lambda$ 5130 at least in part. Reduction of quasar spectra and standard stars followed exactly the same procedures described in Sulentic et al. (2004). Wavelength calibration yielded rms residuals of 0.4, 0.6 and 0.9 Å in the sZ, J and sH windows, respectively. Absolute flux scales of the spectra will be inaccurate because atmospheric seeing almost always exceeded the slit width ( $\approx 0''.6$ ) resulting in significant light loss.

Table 1 summarizes the new observations and the basic format is given below the table. All sources come from the Hamburg-ESO (HE) quasar survey, which is a flux limited (with limiting  $m_B \approx 17.5$ ), color-selected survey (Wisotzki et al., 2000). Column 2 of Table 1 lists the blue apparent magnitudes from the HE survey papers (Reimers et al., 1996; Wisotzki et al., 2000) while Col. 3 lists the source redshift  $z$  computed as described in section 3. The brightest sources of the HE at intermediate redshift were preferentially selected. Col. 4 indicates whether [OIII] $\lambda$ 5007 was used to compute  $z$  as indicative of the source rest frame. The absolute magnitude  $M_B$  reported in Col. 5 was computed by assuming  $H_0 = 70 \text{ km s}^{-1} \text{ Mpc}^{-1}$ , and relative energy density  $\Omega_M = 0.3$  and  $\Omega_\Lambda = 0.7$ . The  $k$  correction was computed for a spectral index  $a = 0.6$  ( $S \propto \nu^{-a}$ ). Col. 6 gives the ratio of log specific fluxes at 6 cm and 4400 Å ( $\log R_k$ ). In most cases only NRAO VLA Sky Survey (NVSS) upper limits are available. Columns 7-12 give details of the observations explained in the footnotes. The continuum  $S/N$  estimate given in Col. 12 was measured using a small region of the spectrum that was as flat and free of line emission as possible.

## 3. Data Analysis

### 3.1. Redshift Determination and Rest Frame Corrections

Small offsets are present in the wavelength calibration, because the arc lamp frames were obtained in daytime, and therefore usually after grism movement. A correction for these shifts was obtained by measuring the centroids of 2-3 OH sky lines against the arc calibration and calculating the average difference, which reached at most 6.5 Å or 2.5 pixels in either direction. Rest frame determination for the 9 new sources was usually estimated from the H $\beta$  peak redshift (assumed rest frame  $\lambda = 4861.33$  Å). [OIII] $\lambda$ 5007 (assumed rest frame  $\lambda = 5006.85$  Å) yielded a consistent measurement in only two sources (where the results were averaged. Two sources show no clear detection of [OIII] $\lambda$ 4959,5007 while the remaining five show a significant disagreement between [OIII] $\lambda$ 5007 and H $\beta_{\text{NC}}$ . In these sources (we call the extreme examples of them “blue outliers”) it is not advisable to use [OIII] $\lambda$ 5007 for redshift determination (Zamanov et al., 2002; Marziani et al., 2003b; Aoki et al., 2005; Boroson, 2005). The adopted estimate was used to deredshift the spectra while the `dopcor` IRAF task applied a  $(1+z)^3$  correction to convert observed specific fluxes into rest frame values. Fig. 1 shows the deredshifted spectra.

### 3.2. Continuum and FeII subtraction

Our spectral analysis made use of standard IRAF tasks with the first step involving continuum modelling and subtraction. Using Chebyshev polynomials of 3<sup>rd</sup> or 2<sup>nd</sup> order, a reasonably smooth continuum subtraction was obtained for all sources. To estimate errors in the continuum assessment introduced by noise, we also defined a minimum and a maximum continuum. Continuum fluxes were chosen at about  $-3\sigma$  (minimum) and  $+3\sigma$  (maximum), where  $\sigma$  is the noise standard deviation from the most likely continuum choice. Errors in continuum placement defined by difference between the extreme continua and the most probable one were then propagated according to standard error theory. The results of this procedure are consistent with continuum fits employing very simple models (Malkan & Sargent, 1982; Shang et al., 2004). We assumed that the continuum underlying the H $\beta$  spectral regions is due to two components: either a blackbody of temperature 25000° K or a power law of slope  $b = 0.7$  ( $f_\nu \propto \nu^{-b}$ ; assumed to be valid only locally around H $\beta$ ). In 5 sources the sole black body component produces a good fit; in 2 the blackbody component is dominant, and only in the remaining 2 cases the power-law alone can provide a good fit. This method has some limitations due to the small spectral bandwidth covered by our spectra, to the relative strength of FeII and to internal reddening effects. Since we did not attempt to change the blackbody temperature nor the slope of the power-law, we adopt the empirical continuum which is visually more accurate.

The emission blends of FeII were subtracted using the template method based upon the spectrum of I Zw 1 (Boroson & Green, 1992; Marziani et al., 2003a). The strongest FeII blends fall in the wavelength ranges 4450–4600 Å (blue blend: FeII $\lambda$ 4570) and 5200–5600 Å (red blend: FeII $\lambda$ 5130). The method includes the following steps: (1) the template intensity is scaled to roughly match the observed spectrum, (2) a Gaussian broadening factor is estimated from FWHM  $H\beta_{\text{BC}}$  (3) a careful estimate of minimum and maximum plausible broadening factor is made to set a reliable  $\pm 3\sigma$  uncertainty and (4) the template intensity is adjusted as necessary after broadening. The resultant template was subtracted from the continuum-subtracted spectra. The blue side of the spectrum including FeII $\lambda$ 4570 is missing, or not fully covered, in several sources (HE 0946–0500, HE 1003+0149, HE 1017–0009, HE 1249–0648 and HE 1258–0823). In these cases the best template fit was achieved for the red blend and a fixed ratio between the red and blue blends was assumed to reproduce FeII $\lambda$ 4570. Fig. 2 shows the estimated FeII emission (green lines). FeII was subtracted before continuum fitting in sources with strong FeII emission.

The [OIII] $\lambda\lambda$ 4959,5007 lines were measured after FeII subtraction and taking into account the following considerations: (1) the flux ratio between [OIII] $\lambda$ 5007 and [OIII] $\lambda$ 4959 should be  $\approx 3$ , (2) both lines should show identical profiles and (3) any  $H\beta_{\text{BC}}$  emission underlying [OIII] $\lambda\lambda$ 4959,5007 is expected to have a smooth shape. Sources HE 1249–0648 and HE 1258–0823 see (Fig. 2) show a small bump at  $\lambda \approx 5016$  Å which is either an FeII subtraction residual or emission from HeI $\lambda$ 5016 (weak redshifted [OIII] $\lambda$ 5007 would be almost unprecedented). After subtraction of  $H\beta_{\text{NC}}$  (following Marziani et al., 2003a), the  $H\beta_{\text{BC}}$  profile was fit with a high order spline function (IRAF task SFIT). This procedure does not yield a model fit but only an empirical fit that smooths the noise and reproduces the main features and inflections in  $H\beta_{\text{BC}}$ .

## 4. Immediate Results

### 4.1. Line Measurements and Uncertainties

**Line Fluxes and Equivalent Widths** Table 3 gives line measurements for the new VLT spectra with the basic format given in the footnote. Cols. 3 and 4 give equivalent width (EW) measures for  $H\beta_{\text{BC}}$  and FeII $\lambda$ 4570 respectively. We evaluated uncertainties associated with the continuum level (derived from the minimum and maximum reasonable continuum estimates) and line flux errors estimated from the  $S/N$ . These estimates were combined quadratically to obtain uncertainties for EW measures. A similar procedure was applied to obtain uncertainty estimates for  $H\beta_{\text{NC}}$  and [OIII] $\lambda\lambda$ 4959,5007. The EW uncertainty for  $H\beta_{\text{NC}}$  was derived from the estimated maximum and minimum possible  $H\beta_{\text{NC}}$  component in the  $H\beta$  line. The relative error of the  $H\beta_{\text{NC}}$  flux can be large (see Table 3) and in some cases an  $H\beta_{\text{NC}}$  component may not be present.

**Fe II $_{\text{opt}}$  width** FeII emission is heavily blended so that widths of individual lines must be obtained from the best broadening parameter that was used for the template fit. This requires that we assume a constant width for all FeII lines which so far appears to be reasonable. FWHM(FeII $\lambda$ 4570) values derived from the template broadening factor are reported in Col. 5 of Table 3. Uncertainty estimates for FWHM(FeII $\lambda$ 4570) were obtained by increasing/decreasing the broadening factor until we could detect significant changes in the best fit. Simulated data reveal that it is possible to estimate the FeII $\lambda$ 4570 width up to FWHM(FeII $\lambda$ 4570)  $\approx 6000$  km s $^{-1}$ . Due to the very large uncertainty of FeII $\lambda$ 4570 width determination for individual sources,  $M_{\text{BH}}$  estimates based on FWHM(FeII $\lambda$ 4570) measures are used mainly for confirmatory purposes of statistical trends detected with  $H\beta$ .

**$H\beta_{\text{BC}}$  Line Profiles** Measurements of FWHM( $H\beta$ ) together with other important line parameters like asymmetry index, kurtosis and line centroid at various fractional intensities were derived using a FORTRAN program developed for that purpose. These parameters are the same as defined in several previous papers (Marziani et al., 1996, 2003a; Sulentic et al., 2004) and are given in Table 3. Each line measure is followed in the next Col. by its appropriate uncertainty. Cols. 2 and 4 give the Full Width at Zero Intensity (FWZI) and FWHM. Col. 6 gives the asymmetry index (AI) as defined in Sulentic et al. (2004). Col. 8 lists kurtosis values while the remaining part of Table 3 lists measures of the  $H\beta_{\text{BC}}$  centroid at various fractional intensities. (in km s $^{-1}$ ). All uncertainties represent the  $2\sigma$  confidence level.

The dichotomy in  $H\beta_{\text{BC}}$  profile shape (and many other properties) between Population A and B (Sulentic et al., 2002) is seen in the new source measures and in the rest of our higher redshift sample (Sulentic et al., 2004). Redward asymmetries (A.I.  $\gtrsim 0.2$ ) are most often found in Pop. B sources. They also show  $H\beta_{\text{BC}}$  profiles that are best fit with Gaussian functions, and some profile appear composite. A few sources appear to deviate from the trend found in previous work that FWHM of  $H\beta_{\text{BC}}$  and the FeII lines are very similar (Marziani et al., 2003a,c). HE 1249-0648 and HE 1258–0823 show FWHM( $H\beta_{\text{BC}}$ )  $\gg$  FWHM(FeII $\lambda$ 4570). While FWHM(FeII $\lambda$ 4570) is subject to large uncertainty, the difference is confirmed by careful reinspection of these spectra. This condition is seen in only 2/215 sources in the Marziani et al. (2003a) sample. Both (IRAS 07598+6508 and Mkn 235) are BAL QSOs which are also FIR ultra-luminous (Sulentic et al., 2006). In addition to a CIV $\lambda$ 1549 BAL with high terminal velocity, these objects have a strong, blueshifted CIV $\lambda$ 1549 emission line component. Blueshifted Balmer emission is probably associated with the high-ionization gas emitting CIV $\lambda$ 1549. The absence of any detectable [OIII] $\lambda\lambda$ 4959,5007 emission, along with a possible HeI feature at  $\lambda$ 5016 Å support the possibility that HE 1249-0648 and HE 1258–0823 could be BAL QSOs similar to IRAS

07598+6508 and Mkn 235. Further support comes from an inspection of the HE survey spectra of both objects which indeed show blueshifted broad absorption in the MgII $\lambda$ 2800 line.

## 5. Black Hole Mass and Eddington Ratio

### 5.1. Basic Equations

One can write the velocity dispersion  $v$  in Eq. 1 as  $v \approx \sqrt{3}/2 \text{ FWHM}(\text{H}\beta_{\text{BC}})$  in the case of randomly oriented velocities projected along the line-of-sight. The expression for black hole mass is then:

$$M_{\text{BH}} \approx \frac{3}{4} \frac{r_{\text{BLR}} \text{FWHM}(\text{H}\beta_{\text{BC}})^2}{G} \quad (3)$$

In the absence of reverberation data one must rely on the correlation between reverberation radius and source luminosity  $r_{\text{BLR}} \propto (L_{5100})^\alpha$ , where  $L_{5100}$  is the specific luminosity at  $\lambda \approx 5100 \text{ \AA}$  (Kaspi et al., 2000, 2005). This formula relates BLR distance from the central continuum source and specific luminosity ( $\text{ergs s}^{-1} \text{ \AA}^{-1}$ ) near  $5100 \text{ \AA}$ . Following Kaspi et al. (2005) one can write:

$$r_{\text{BLR}} \approx 0.697 \cdot 10^{17} \cdot \left[ \frac{\lambda L_\lambda (5100 \text{ \AA})}{10^{44} \text{ erg s}^{-1}} \right]^{0.67} \text{ cm} \quad (4)$$

We can make two estimates of  $M_{\text{BH}}$  using these relationships assuming two different values for  $\lambda L_\lambda$ . The first method derives  $M_{\text{B}}$  from tabulated values of  $V$  or  $B$  apparent magnitudes:

$$\lambda L_\lambda (5100 \text{ \AA}) \approx 3.14 \cdot 10^{35-0.4(M_{\text{B}})} \text{ ergs s}^{-1} \quad (5)$$

A second possibility involves estimating the specific luminosity near  $5100 \text{ \AA}$  directly from flux measures using the adopted continuum fits for our spectra. More explicitly  $\lambda L_\lambda$  is computed as follows:

$$\lambda L_\lambda (5100 \text{ \AA}) = 4\pi d_{\text{P}}^2 \lambda f_\lambda (5100 \text{ \AA}) \text{ ergs s}^{-1}, \quad (6)$$

where  $d_{\text{P}}$  is the redshift derived distance and  $f_\lambda$  is the specific flux in the rest frame at  $5100 \text{ \AA}$  (after correction for Galactic extinction  $A_{\text{B}}$  at the observed wavelength). The second choice has the advantage that the continuum  $f_\lambda$  and  $\text{FWHM}(\text{H}\beta_{\text{BC}})$  are measured from the same spectrum. Expected light losses are estimated to be  $\approx 35 \%$  of the quasar flux with average Paranal seeing ( $0.''6$ ). We apply this average correction to the observed flux before computing  $M_{\text{BH}}$ .

Substituting the expression for  $r_{\text{BLR}}$  in the mass formula one obtains the following relation:

$$M_{\text{BH}} \approx 5.48 \cdot 10^6 \left[ \frac{\lambda L_\lambda (5100 \text{ \AA})}{10^{44} \text{ erg s}^{-1}} \right]^{0.67} \left( \frac{\text{FWHM}(\text{H}\beta_{\text{BC}})}{1000 \text{ km s}^{-1}} \right)^2 \quad (7)$$

where  $M_{\text{BH}}$  is in solar mass units ( $M_\odot$ ).

Fig. 3 shows the distribution of  $M_{\text{BH}}$  as a function of  $z$ .  $M_{\text{BH}}$  estimates are based on the  $\text{FWHM}(\text{H}\beta_{\text{BC}})$  measures

reported in Table 2. All sources with  $z \gtrsim 0.8$  are from the VLT sample. We do not show  $M_{\text{BH}}$  values derived from  $M_{\text{B}}$  as in Marziani et al. (2003b) for clarity, since they basically confirm the same trends obtained from the specific fluxes.

### 5.2. Improved $M_{\text{BH}}$ Estimators?

As briefly summarized in §1, there is some evidence suggesting that the virial assumption is reasonable for LILs in a significant fraction of quasars (Population A; about 50-60% of low  $z$  quasars). Our VLT spectra confirm that any dependence of  $\text{FWHM}(\text{H}\beta_{\text{BC}})$  on source luminosity is weak (Sulentic et al., 2004). Table 3 suggests that low redshift trends for asymmetries and line shifts are preserved in the intermediate  $z$  sample. It is therefore not certain that  $\text{FWHM}(\text{H}\beta_{\text{BC}})$  is a valid estimator of the virial velocity for all sources even after proper  $\text{H}\beta_{\text{NC}}$ ,  $[\text{OIII}]\lambda\lambda 4959, 5007$ , FeII subtraction.

A more physical approach to  $M_{\text{BH}}$  estimation uses the FWHM of the variable part of the  $\text{H}\beta_{\text{BC}}$  profile (Peterson et al., 2004). Fig. 4 plots  $\text{FWHM}_{\text{rms}}$  values from Peterson et al. (2004) versus our  $\text{FWHM}(\text{H}\beta_{\text{BC}})$  measures (Marziani et al., 2003a) for all sources in common. Sources with  $\text{FWHM} \lesssim 4000 \text{ km s}^{-1}$  show a correlation while the situation is less clear for sources with  $\text{FWHM} \gtrsim 4000 \text{ km s}^{-1}$ . We recall that this value indicates the nominal population A-B boundary (Sulentic et al., 2000b) that emerged in our E1 studies. A least-square best fit analysis yields a ‘‘corrected’’  $\text{FWHM}(\text{H}\beta_{\text{BC}})$  estimate:  $\text{FWHM}^{\text{corr}}(\text{H}\beta_{\text{BC}}) \approx -710(\pm 800) + 1.13(\pm 0.28) \text{ FWHM}(\text{H}\beta_{\text{BC}})$  for  $\text{FWHM} \lesssim 4000 \text{ km s}^{-1}$  and  $\text{FWHM}^{\text{corr}}(\text{H}\beta_{\text{BC}}) \approx 650(\pm 1000) + 0.79(\pm 0.14) \text{ FWHM}(\text{H}\beta_{\text{BC}})$  for  $\text{FWHM} \gtrsim 4000 \text{ km s}^{-1}$ . The slope depends somewhat on the fitting method (a robust fit yields 0.94 and 0.72) but is always less steep for  $\text{FWHM} \gtrsim 4000 \text{ km s}^{-1}$ . An immediate implication is that optically thick BLR gas responding to continuum changes shows a velocity dispersion correlated with – but slightly lower than that of the integrated profile at all FWHM.

A break in the linear fit at  $4000 \text{ km s}^{-1}$  is consistent with several previous findings: (a) mean and possibly systematic  $\text{H}\beta_{\text{BC}}$  profile differences between Pop. A and B sources (Sulentic et al., 2002); (b) the lack of strong profile changes in Pop. A sources (Giveon et al., 1999); (c) profile asymmetries frequently observed in Pop. B sources. They might represent a distinct redshifted emission component (Sulentic et al., 2002) which may arise in less optically thick gas than the rest of the  $\text{H}\beta_{\text{BC}}$  profile (Sulentic et al., 2000c). If the redshifted component is emitted in an innermost VBLR, the FWHM of the whole  $\text{H}\beta_{\text{BC}}$  profile is obviously increased over the value due to the line component that is actually responding, and that is most likely located farther away from the central continuum source. Even if the virial assumption holds for the VBLR (but the frequent asymmetries warn us that this might not be the case), the use of the FWHM from the

whole H $\beta_{\text{BC}}$  profile and of  $r_{\text{BLR}}$  from the reverberating part, yields an  $M_{\text{BH}}$  overestimate. This interpretation of the correlations in Fig. 4 is advanced with caution because of the small sample size and especially because of the poor statistics for sources with FWHM  $\gtrsim 4000 \text{ km s}^{-1}$ . It is also possible to produce a meaningful fit with a second-order polynomial. We apply a tentative correction to the FWHM measures FWHM $^{\text{corr}}$ (H $\beta_{\text{BC}}$ ) and therefore to resultant  $M_{\text{BH}}$  estimates using the second-order fit shown in Fig. 4 which approximates very well the linear trends.

If an optically thin/nonvirialized component is present in the H $\beta_{\text{BC}}$  profile of many sources then we might use as a virial estimator the FWHM of a line, or lines, arising in BLR gas but not likely to be present in the VBLR region. FWHM(FeII $\lambda$ 4570) is an obvious alternative because there is no evidence for a VBLR emission component in the broad FeII blends. It is not strictly correct to use it because the  $r_{\text{BLR}}-L_{\lambda}$  relation was deduced for H $\beta$ . The most serious difficulty lies in obtaining a reliable FWHM(FeII $\lambda$ 4570) estimate from the heavily blended FeII emission. Considering the EW and FWHM limits for detection of Fe II $_{\text{opt}}$  emission (Marziani et al., 2003a) we conclude that a reasonable FWHM measurement is possible for  $\approx 120$  sources in our low  $z$  spectral atlas. Measurement uncertainties for FWHM(FeII) will be larger than for FWHM(H $\beta_{\text{BC}}$ ) and are estimated to lie between 20–50%. The best fit of FWHM(FeII $\lambda$ 4570) vs. FWHM(H $\beta_{\text{BC}}$ ) ( $\text{km s}^{-1}$ ) is consistent with FWHM(FeII $\lambda$ 4570)  $\approx$  FWHM(H $\beta_{\text{BC}}$ ) for FWHM(H $\beta_{\text{BC}}$ )  $\lesssim 4000 \text{ km s}^{-1}$ , while it is FWHM(FeII $\lambda$ 4570)  $\approx 0.67 \cdot$  FWHM(H $\beta_{\text{BC}}$ ) +  $820 \text{ km s}^{-1}$  if FWHM(H $\beta_{\text{BC}}$ )  $\gtrsim 4000 \text{ km s}^{-1}$ .

The relationship between FWHM(H $\beta_{\text{BC}}$ ) and FWHM(FeII) confirms that individual FeII lines show approximately the same width as H $\beta_{\text{BC}}$  and as the rms H $\beta_{\text{BC}}$  component implying a common kinematic environment if FWHM(H $\beta_{\text{BC}}$ )  $\lesssim 4000 \text{ km s}^{-1}$ . If FWHM(H $\beta_{\text{BC}}$ )  $\gtrsim 4000 \text{ km s}^{-1}$ , FWHM(FeII) follows a trend closer to that of the rms H $\beta_{\text{BC}}$  component. Therefore if the rms H $\beta_{\text{BC}}$  component arises from gas in virialized motion, the same can be reasonably assumed for the whole FeII $\lambda$ 4570 emission.

### 5.3. $M_{\text{BH}}$ and $L/L_{\text{Edd}}$ Dependence on Redshift

#### 5.3.1. $M_{\text{BH}}$

Fig. 3 shows the distribution with  $z$  of  $M_{\text{BH}}$  estimates derived using uncorrected FWHM(H $\beta_{\text{BC}}$ ) measures. This can be compared with Fig. 5 where we show corresponding distributions of  $M_{\text{BH}}$  derived using corrected FWHM $^{\text{corr}}$ (H $\beta_{\text{BC}}$ ) measures and using FWHM(FeII $\lambda$ 4570). FWHM $^{\text{corr}}$ (H $\beta_{\text{BC}}$ ) values were derived from the second-order relation in Fig. 4.

The distribution of data points in the log  $M_{\text{BH}}$  vs.  $z$  plane reflects selection effects intrinsic to any flux limited sample. If we consider AGNs that are radiating at a given  $L/L_{\text{Edd}}$  we easily obtain  $M_{\text{BH}}$  for a given apparent magnitude:

$$M_{\text{BH},9\text{G}} = 3.85 \cdot 10^6 h^{-2} \left( \frac{L}{L_{\text{Edd}}} \right)^{-1} \cdot 10^{-0.4m_{\text{B}}} \cdot [1.5 (1 - e^{-\frac{z}{6.107}}) + (1 - e^{-\frac{z}{1.266}})]^2 \cdot (1+z)^{(1-a)}.$$

Appendix B details how Eqn. 8 was derived. If we adopt a limiting magnitude  $m_{\text{B}} \approx 17.5$  (appropriate for the Hamburg-ESO survey) and consider a maximum Eddington ratio  $L/L_{\text{Edd}} \approx 1$  we obtain the minimum  $M_{\text{BH}}$  detectable as a function of  $z$ . Limiting  $M_{\text{BH}}$  curves are shown in Fig. 3, Fig. 5, and Fig. 6.

All sources show  $M_{\text{BH}} \gtrsim 10^6 M_{\odot}$ . In the range  $1 \lesssim z \lesssim 2.5$  we begin to find a significant black hole population in the range  $\sim 10^{9.5} M_{\odot} \lesssim M_{\text{BH}} \lesssim 10^{10} M_{\odot}$ . If we consider  $M_{\text{BH}}$  values derived from FeII $\lambda$ 4570 as well as from FWHM $^{\text{corr}}$ (H $\beta_{\text{BC}}$ ) (Fig. 5, open and filled symbols respectively) we get a somewhat different picture. Almost all sources lie below  $\approx 5 \cdot 10^9 M_{\odot}$  (all sources with  $z \lesssim 1$ ); only three sources whose  $M_{\text{BH}}$  has been computed with from FWHM $^{\text{corr}}$ (H $\beta_{\text{BC}}$ ) lie significantly above this limit. Our sample of intermediate  $z$  quasars with compatible quality data is still small so caution is needed. It should be pointed out that the use of H $\beta_{\text{BC}}^{\text{corr}}$  is self-consistent, since no H $\beta$  surrogate line was used.

The upper panel of Fig. 6 identifies sources on the basis of radio-loudness where open and solid symbols denote radio-loud (RL; see definition in Sulentic et al., 2003) and radio-quiet (RQ) sources respectively. At low  $z$  RQ sources are distributed across the full range of  $M_{\text{BH}}$  up to  $M_{\text{BH}} \gtrsim 10^9 M_{\odot}$ , although RL sources tend to have larger  $M_{\text{BH}}$  (Metcalf & Magliocchetti, 2006; Marziani et al., 2003b, and references therein). The same consideration apply to Pop. A and Pop. B sources (lower panel of Fig. 6), and this is not surprising since most Pop. A sources are RQ. At intermediate  $z$ , selection effects limit the detectable black holes to  $M_{\text{BH}} \gtrsim 10^9 M_{\odot}$ , so that only the high end of the quasar  $M_{\text{BH}}$  distribution can be traced. It is too early to decide whether systematic differences in the  $M_{\text{BH}}$  distribution of RQ and RL sources may still exist at intermediate  $z$ , at least from the present data.

#### 5.3.2. $L/L_{\text{Edd}}$

Fig. 7 shows the distribution of  $L/L_{\text{Edd}}$  estimates as a function of  $z$ . A preliminary analysis in terms of  $L/L_{\text{Edd}}$ , and including discussion of bolometric luminosity estimation, was presented in Marziani et al. (2003b).

The existence of apparently super-Eddington radiators in the low- $z$  part of Fig. 7 involves the most extreme NLSy1 sources. One caveat about interpreting any of them as super-Eddington involves the significant uncertainties associated with these estimates. If we assume a typical uncertainty of  $\pm 50\%$  for the bolometric correction (neglecting beaming or lensing) and  $\pm 10\%$  for the virial estimator (basically the uncertainty in the FWHM measurement) we

find a  $\Delta \log L/L_{\text{Edd}} \approx 0.13$  (neglecting the scatter in Eqn. 2). A serious source of uncertainty ignored until now involves source orientation with respect to the line-of-sight. The virial velocity dispersion that H $\beta_{\text{BC}}$  is assumed to measure is now widely assumed to involve Keplerian rotation in an accretion disk or in a flattened distribution near the disk. If our candidate super-Eddington sources are mostly viewed with (face-on disk and/or pole-on jet) then  $M_{\text{BH}}$  can be significantly underestimated. An orientation correction applied to extreme NLSy1 sources (we call them Pop. A “blue outliers”) interpreted as face-on, will move them below  $L/L_{\text{Edd}} \approx 1$  (Marziani et al., 2003b, see arrows in their Figure 12). At high  $z$  we so far find no strong evidence for any super-Eddington sources. The thick solid line in Fig. 7 shows the expected  $L/L_{\text{Edd}}$  detection limit deduced from Eqn. 8 for a flux-limited survey ( $m_{\text{B}} \approx 17.5$ ) and a quasar with  $M_{\text{BH}} \approx 4 \cdot 10^9 M_{\odot}$ . All quasars in our sample fall above the minimum detectable  $L/L_{\text{Edd}}$ , suggesting that masses larger than  $\approx 4 \cdot 10^9 M_{\odot}$  are not strictly necessary from our data (see §6.1 for further discussion).

A physical basis for the dichotomy between Pop. A and Pop. B (Sulentic et al., 2000b; Marziani et al., 2001, 2003b) is supported by this analysis in the sense that Fig. 4 shows evidence for a change at about  $\text{FWHM}(\text{H}\beta_{\text{BC}}) \approx 4000 \text{ km s}^{-1}$ . Fig. 7 identifies Pop. A and B sources as filled and open symbols respectively. Here we apply the luminosity-dependent definition of the Pop. A-B boundary as defined in Fig. 6 of Sulentic et al. (2004). It shows that the Eddington ratio of Pop. A sources is systematically larger than that of Pop. B, and that the apparent boundary between the two populations may increase with redshift. If we focus on the intermediate  $z$  quasars then Pop. A sources show an average  $L/L_{\text{Edd}} \approx 0.78$  compared to 0.27 for 10 Pop. B sources. Even these small samples of Pop. A and B sources show significantly different  $L/L_{\text{Edd}}$  distributions according to a Kolmogorov-Smirnov (K-S) test. RL AGNs are systematically low  $L/L_{\text{Edd}}$  radiators since they are almost entirely Pop. B sources.

It is interesting to note that with: (1) a limiting magnitude  $m_{\text{B}} \approx 16.5$ , (2)  $L/L_{\text{Edd}} \lesssim 1$  and (3)  $M_{\text{BH}} \lesssim 4 \cdot 10^9 M_{\odot}$  we should detect fewer sources beyond  $z \approx 2$  (no source below the dot-dashed curve of Fig. 7). If our assumptions about the quasar bolometric correction are valid up to that redshift, selection effects may influence the relative frequency of Pop. A and B sources (the two Populations have different  $L/L_{\text{Edd}}$  distributions) rather than the intrinsic properties of LILs. In this case selection effects on  $L/L_{\text{Edd}}$  should strongly influence the so-called “Baldwin effect” involving CIV $\lambda$ 1549 and other HILs (Bachev et al., 2004, and references therein) because CIV $\lambda$ 1549 is more prominent in Pop. B, and Pop. B sources are more easily lost at high  $z$ .

## 6. Discussion

The present paper provides  $M_{\text{BH}}$  estimates that have three advantages: (1) a consistent data analysis procedure is em-

ployed over the entire redshift range  $0.0 \lesssim z \lesssim 2.5$  by using the same  $M_{\text{BH}}$  tracer, H $\beta_{\text{BC}}$ ; (2)  $S/N$  and resolution of the spectroscopic data sample are high enough to permit a careful study of the H $\beta_{\text{BC}}$  profile, and (3) the data quality allows reasonable estimates of FWHM FeII in many of the sources.

### 6.1. What are the largest black hole masses?

Netzer (2003) discussed several problems with  $M_{\text{BH}} \gtrsim 10^{10} M_{\odot}$ . If the black hole mass vs. bulge mass ( $M_{\text{bulge}}$ ) relation (Ferrarese & Merritt, 2000) is valid at high  $z$  then  $M_{\text{BH}} \sim 10^{10} M_{\odot}$  would imply stellar velocity dispersion  $\sigma_{\star} \approx 700 \text{ km s}^{-1}$  (following Gebhardt et al., 2000) and resultant bulge masses  $M_{\text{bulge}} \gtrsim 10^{13} M_{\odot}$  which are not observed at low- $z$  (McLure & Jarvis, 2004; Netzer, 2003; Wang, 2003). Recent results for the fundamental plane of elliptical galaxies, and the most massive spheroids at  $z \lesssim 0.3$  from Sloan Digital Sky Survey measures, confirm that  $\sigma_{\star} \lesssim 500 \text{ km s}^{-1}$  (SDSS, Bernardi et al., 2003, 2005, all galaxies with  $\sigma \gtrsim 500 \text{ km s}^{-1}$  are likely due to chance superposition).

There are several proposed interpretations of this problem: (1) the  $M_{\text{BH}} - M_{\text{bulge}}$  relationship may not strictly hold for all hosts, (2) the virial assumption is not applicable, (3) results are plagued by such large uncertainties – including the one of the luminosity index  $\alpha$  – that very large mass estimates are not real (Vestergaard, 2002), and (4) some systematic effects may not have been considered.

#### 6.1.1. The $M_{\text{BH}} - M_{\text{bulge}}$ Relationship

Nuclei with  $M_{\text{BH}} \gtrsim 5 \cdot 10^9 M_{\odot}$  are not observed in galaxies of the local Universe if a direct black hole mass determination is possible from circum-nuclear kinematics (Marconi & Hunt, 2003). They are expected to be rare and difficult to find, considering also that they should be in a dormant or nearly dormant stage at the present epoch. Integrating the quasar luminosity function at  $z \approx 1.5$  (Boyle et al., 2000), we find a comoving density of quasars above the HE limiting magnitude (which corresponds to  $M_{\text{B}} \approx -27.1$  for a  $k$ -correction  $a = 0.6$ )  $\sim 3 \cdot 10^{-8} \text{ Mpc}^{-3}$ . This indicates that the present-day density of the most massive black holes that were once luminous quasars should be very low,  $\sim 2 \cdot 10^{-9} \text{ Mpc}^{-3}$ . Even so, they should be much more frequent than the very massive spheroids that would host them if the  $M_{\text{BH}} - M_{\text{bulge}}$  relationship is valid. To estimate the density of spheroids with  $\sigma_{\star} \gtrsim 500 \text{ km s}^{-1}$ , one must extrapolate the  $\sigma$  distribution function provided by Sheth et al. (2003) to unobserved domains in  $\sigma$ . Integrating the Sheth et al. (2003) function for  $\sigma_{\star} \gtrsim 500 \text{ km s}^{-1}$ , one obtains that the comoving density of all local spheroids is three orders of magnitude lower ( $\sim 6 \cdot 10^{-13} \text{ Mpc}^{-3}$ ) than that of the most massive black holes. A possible implication is that the  $M_{\text{BH}} - M_{\text{bulge}}$  relation is not linear or of universal validity, i.e. some galaxies host larger black hole masses

than expected. This conclusion should remain valid also at intermediate redshifts. A constant  $M_{\text{BH}}/M_{\text{bulge}}$  ratio cannot hold forever if bulge mass grows by secular evolutionary processes. Evolution goes in the sense that the spheroids may increase their masses at a later cosmic age ( $z \lesssim 2$ ; Treu et al., 2004; Peng et al., 2005) significantly more than their central black hole: the most massive black hole should be already “brightly shining” at  $z \approx 2$  (McLure et al., 2005, and references therein). A nonlinear  $M_{\text{BH}} - M_{\text{bulge}}$  relation has been proposed (Laor, 2001) for local hosts, with  $M_{\text{BH}}$  accounting for only 0.05 % of the bulge mass in low-luminosity galaxies and 0.5 % in giant ellipticals. In this case,  $M_{\text{BH}} \sim 10^{10} M_{\odot}$  would imply  $M_{\text{bulge}} \sim 10^{12} M_{\odot}$ , which is at the upper end of the spheroid masses measured locally (Marconi & Hunt, 2003).

The problem can be made to disappear if  $M_{\text{BH}} \lesssim 3 \cdot 10^9 M_{\odot}$ . Bernardi et al. (2005) find a maximum  $\sigma_{\star} \approx 500 \text{ km s}^{-1}$ . These local galaxies (with expected  $M_{\text{BH}} \approx 3 \cdot 10^9 M_{\odot}$ ) may have been the hosts of the luminous quasars at  $1 \lesssim z \lesssim 2$  since the number density of spheroids with  $\sigma_{\star} \gtrsim 350 \text{ km s}^{-1}$  is  $\sim 4 \cdot 10^{-7} \text{ Mpc}^{-3}$ , still somewhat larger than the present-day density of supermassive black holes that were radiating at  $M_{\text{B}} \lesssim -25$  ( $\sim 10^{-7} \text{ Mpc}^{-3}$ ).

The curves in Fig. 7, where  $M_{\text{BH}} \sim 4 \cdot 10^9 M_{\odot}$  has been assumed, suggest that there is no need for  $M_{\text{BH}} \gtrsim 10^{10} M_{\odot}$  at  $z \lesssim 2.5$ . Similarly the brightest HE sources in the redshift range  $1 \lesssim z \lesssim 2$  ( $m_{\text{B}} \approx 15.0$  at  $z \approx 1.7$ ) are consistent with  $L/L_{\text{Edd}} \approx 1$  if  $M_{\text{BH}} \sim 4 \cdot 10^9 M_{\odot}$ . In other words, if  $M_{\text{BH}} \sim 10^{10} M_{\odot}$ , then a source at  $L/L_{\text{Edd}} \approx 1$  would be brighter than the brightest quasars observed in the range  $1 \lesssim z \lesssim 2$  (if  $H_0$  is close to the value assumed in this paper).

### 6.1.2. Could A Non-virial Component Yield a Huge $M_{\text{BH}}$ ?

One might envision a non-virial component that increases with source luminosity and systematically broadens the  $\text{H}\beta_{\text{BC}}$  profile. In our so-called Pop. A sources, the high ionization wind that can dominate  $\text{CIV}\lambda 1549$  emission might reasonably be expected to produce Balmer line emission as well. Such an additional (blueshifted) component on the  $\text{H}\beta_{\text{BC}}$  profile would increase FWHM measures (Sulentic et al., 2006, HE 1249–0648 and HE 1258–0823 may show this effect). One intriguing possibility is that high-luminosity sources are extreme Pop. A sources which is supported by models invoking a radiation pressure driven wind. Such an effect would make the correction ( $\sim 500 \text{ km s}^{-1}$ ) deduced for low- $z$  Pop. A sources inadequate. At the other extreme, strong redward asymmetries observed in Pop. B sources indicate that the integrated profile may be affected by gravitational redshift and non-virial motions (Marziani et al., 2003b). A quantitative analysis of these suggestions needs careful analysis beyond the scope of this paper, but in both cases any correction would lower  $M_{\text{BH}}$ .

### 6.1.3. Statistical Errors

It is interesting to consider in more detail the sources that show  $M_{\text{BH}} \sim 10^{10} M_{\odot}$  in our sample. HE 0248–3628 with the largest estimated  $M_{\text{BH}}$  is also one of the highest  $L/L_{\text{Edd}}$  radiators with  $L/L_{\text{Edd}} \sim 1$ . It shows an anomalously large (by a factor  $\sim 10$ ) flux with respect to our other VLT sources which makes it an extremely luminous quasar ( $M_{\text{B}} \lesssim -30$ ; see Sulentic et al., 2004). It falls near the Pop. A–B boundary in Eigenvector 1 space and is a borderline radio-loud source by our definition (Sulentic et al., 2003). It disappears as an outlier if the  $M_{\text{BH}}$  estimated from the tabulated  $M_{\text{B}}$  is adopted. HE 2355–4621 is a second source with  $M_{\text{BH}} \sim 10^{10} M_{\odot}$ . It behaves like a normal radio-quiet Pop. B source. The  $\text{H}\beta_{\text{BC}}$  profile shows a prominent redward asymmetry, which is strongly affecting the width at half maximum. It is also interesting to consider HE 1104–1805, which is the most luminous source in our new sample with ( $M_{\text{B}} \approx -29.5$ ). It behaves like an ordinary Pop. A source and shows  $M_{\text{BH}} \approx 5 \cdot 10^9 M_{\odot}$  which may be overestimated if the continuum is lens brightened (Appendix A).

The high-mass wing of the  $M_{\text{BH}}$  distribution in the redshift range  $1 \lesssim z \lesssim 2$  is consistent with the wing of a Gaussian peaked at  $\approx 3 \cdot 10^9 M_{\odot}$  and dispersion  $\Delta \log M_{\text{BH}} \approx 0.3$  if  $M_{\text{BH}}$  is computed from  $\text{FWHM}^{\text{corr}}(\text{H}\beta_{\text{BC}})$  ( $4 \cdot 10^9 M_{\odot}$  if no correction to  $\text{H}\beta_{\text{BC}}$  is applied). The Gaussian dispersion is consistent with the estimated errors of individual measurements.  $K - S$  tests do not favor significantly different peak masses or a much different dispersion. This suggests that sources with  $M_{\text{BH}} \gtrsim 3 \cdot 10^9 M_{\odot}$  of our data might be mostly due to random errors associated to the uncertainty in individual  $M_{\text{BH}}$  measurements.

### 6.1.4. Systematic Effects

A first systematic effect considers the uncertainty in the index  $\alpha$ . Our  $M_{\text{BH}}$  estimates show the onset of  $M_{\text{BH}} \gtrsim 3 \cdot 10^9 M_{\odot}$  at  $z \sim 0.8$ ; at  $z \gtrsim 0.8$  we observe some of the most luminous HE quasars. The high luminosity range of the Kaspi et al. (2005) relationship remains poorly sampled: there are just 2-3 sources in the range  $45 \lesssim \log \lambda L_{\lambda} \lesssim 46$  (to which most of our intermediate  $z$  sources belong), creating a sample bias and making the correlation analysis intrinsically unstable. In addition, a recent reanalysis of the  $r_{\text{BLR}} - \lambda L_{\lambda}$  correlation suggests a value of  $\alpha$  as low as 0.5 (Vestergaard & Peterson, 2006). If  $\alpha$  is overestimated by  $\Delta \alpha \approx 0.17$  over a luminosity range of  $\sim 10$ ,  $M_{\text{BH}}$  may be overestimated by  $\Delta \log M_{\text{BH}} \approx 0.2$  in our intermediate  $z$  sources.

Pop. A sources show good evidence that LILs are emitted in a strongly flattened system, probably an accretion disk or gas co-planar with the disk.  $\text{CIV}\lambda 1549$  in these sources seems to be dominated by a wind component (Bachev et al., 2004). If these considerations apply also to Pop. B sources (but it is by no means clear, given the large  $\text{FWHM}(\text{H}\beta_{\text{BC}})$  of sources believed to be observed



pole-on) and if the maximum angle between disk axis and line-of-sight is  $\approx 45^\circ$ , a correction could imply a factor  $\lesssim 2$  systematic increase in  $M_{\text{BH}}$ . However, these consideration of orientation effects may not even reopen the problem of very large  $M_{\text{BH}}$  values: if our suggestion of a maximum  $M_{\text{BH}} \approx 3 \cdot 10^9 M_\odot$  is appropriate, taking into account the systematic orientation effects would yield a maximum  $M_{\text{BH}} \approx 6 \cdot 10^9 M_\odot$  which is still plausible. The result that  $L/L_{\text{Edd}} \lesssim 1$  at  $z \gtrsim 0.8$  would be reinforced by systematic orientation effects.

Summing up, our data suggest that very large masses  $\sim 10^{10} M_\odot$  may be not be real, and may be predominantly due to statistical errors and emission line profile broadening that is in part non-virial. The data presented in this paper are consistent with  $M_{\text{BH}}$  not exceeding  $3 \cdot 10^9 M_\odot$  for our sources if the correction to  $\text{FWHM}(\text{H}\beta_{\text{BC}})$  described earlier is applied.

## 6.2. The Best $M_{\text{BH}}$ Estimators

LILs like  $\text{MgII}\lambda 2800$  and  $\text{FeII}$  may yield more reliable results than  $\text{H}\beta_{\text{BC}}$ . HI Balmer line emission can be substantial from gas in a variety of physical conditions. In Pop. B sources, a very broad component may increase the FWHM of the integrated  $\text{H}\beta_{\text{BC}}$  profile (also mimicked by low  $S/N$  data; McIntosh et al., 1999; Shemmer et al., 2004). This very broad component may be optically thin to the ionizing continuum, and therefore non-responsive to continuum changes. The  $\text{H}\beta_{\text{BC}}$  profile of Pop. A sources may be affected by a high-ionization component mentioned earlier.  $\text{FeII}$  is thought to be emitted in a region very optically thick to Lyman continuum which is probably photoionized (Vestergaard & Peterson, 2005; Wang et al., 2005), as the part of  $\text{H}\beta_{\text{BC}}$  responding to continuum changes should be. It is not surprising that the reverberating part of  $\text{H}\beta_{\text{BC}}$  and  $\text{FeII}$  provides width estimates which are consistent, since they are expected to measure the width of a similar sub-region within the BLR. Similar considerations apply to  $\text{MgII}\lambda 2800$  (Wills et al., 1985) since  $\text{MgII}\lambda 2800$  should be mainly emitted in the same zone as  $\text{FeII}$ . McLure & Dunlop (2004) present virial  $M_{\text{BH}}$  estimates for  $\approx 13000$  quasars in the redshift interval  $0.1 \lesssim z \lesssim 2.1$  based on spectra from the SDSS first data release. The mean  $M_{\text{BH}}$  increases with increasing redshift basically as shown in Fig. 3. The mass values found by them are also consistent with a limiting  $M_{\text{BH}}$  around  $3 \cdot 10^9 M_\odot$ , with large scatter. They use  $\text{FWHM}(\text{H}\beta_{\text{BC}})$  or  $\text{FWHM}(\text{MgII}\lambda 2800)$  and find a consistency between the most massive at  $z \approx 2$  and those at  $z \approx 0$ . Given measurement difficulties, and doubts about the virial assumption for most other lines, corrected measures for  $\text{H}\beta_{\text{BC}}$ ,  $\text{FeII}$ , and  $\text{MgII}\lambda 2800$  may offer the best hope for reliable  $M_{\text{BH}}$  and  $L/L_{\text{Edd}}$  estimates out to  $z \approx 2.5$ .

## 7. Conclusions

Nine intermediate  $z$  VLT/ISAAC spectra with high resolution and  $S/N$  supplement an earlier sample of 17 sources. Emission line measurements on  $\text{H}\beta_{\text{BC}}$  and  $\text{FeII}$  presented in this paper strengthen the conclusion of Sulentic et al. (2004) that luminosity effects are weak or absent in the low-ionization lines of AGNs. Results on the  $\text{H}\beta_{\text{BC}}$  profile are consistent with the population A-B hypothesis and Eigenvector 1 parameter space concept developed for low  $z$  AGNs. We computed virial masses and Eddington ratios for the 25 intermediate- $z$  objects plus about 280 lower  $z$  sources, using the same emission line over the entire redshift range for the first time.

We also have how the distributions of  $M_{\text{BH}}$  and  $L/L_{\text{Edd}}$  vs.  $z$  are shaped by selection effects intrinsic to any flux-limited survey at the low  $M_{\text{BH}}$  end. At the high  $M_{\text{BH}}$  end, masses exceeding a few  $10^9 M_\odot$  may be rare if corrections for non-virial broadening and statistical errors are taken into account. This suggestion is based on just 25 objects distributed over the entire redshift range  $0.9 \lesssim z \lesssim 2.5$ . Confirmation from a larger sample of intermediate- $z$  observations is needed.

*Acknowledgements.* We thank a referee for many useful suggestions and the tenacity to ensure that they were taken into account. We also thank Lutz Wisotzki for providing us with the HE optical spectra. D. D-H, and JS acknowledge financial support from grant IN100703 from PAPIIT, DGAPA, UNAM.

## Appendix A: Notes on Individual Sources

### A.1. HE0512-3329

HE 0512-3329 was discovered as a probable gravitationally lensed quasar with the Space Telescope Imaging Spectrograph (STIS). It is a doubly imaged QSO with a source redshift of  $z = 1.58$  and an image separation of  $0''.644$ . The flux ratio  $\frac{A}{B}$  of the lensed images shows a strong dependence on wavelength. In the R and I bands, A is brighter than B by about 0.45 mag while the two are almost equal in the band B. For smaller wavelengths, especially close to the limit near  $2000 \text{ \AA}$ , B becomes much brighter than A by about 1.3 mag. A natural explanation for this effect is differential reddening caused by different extinction effects in the two lines of sight (Gregg et al., 2000). Microlensing by stars and other compact object in the lensing galaxy also plays a role in this source (Wucknitz et al., 2003). Unfortunately, the small separation does not allow to us to distinguish component A and B on the ISAAC spectrum. The HE 0512-3329 acquisition image is compatible with an unresolved source. Considering the flux ratios in the R and I band, it is reasonable to assume that our spectrum is dominated by the A component.

### A.2. HE1104-1805

HE 1104-1805 is a double-image lensed quasar discovered by Wisotzki et al. (1993). The image separation is  $\Delta\theta = 3''.19$ , the source redshift is  $z_s = 2.319$ , and the lens redshift is  $z_l = 0.729$ . Wisotzki et al. (1995) reported that the continuum flux in both images is highly variable but that the line fluxes do not change, as expected if microlensing is operating. On the acquisition image of HE 1104 there is a second source at  $3.5''$  but it is completely off-slit.

**Table 1.** Basic Properties of Sources and Log of Observations

Object name (1)	$m_{\text{B}}^{\text{a}}$ (2)	$z^{\text{b}}$ (3)	Line <sup>c</sup> (4)	$M_{\text{B}}^{\text{d}}$ (5)	$\log R_{\text{K}}^{\text{e}}$ (6)	Date <sup>f</sup> (7)	Band <sup>g</sup> (8)	DIT <sup>h</sup> (9)	$N_{\text{exp}}^{\text{i}}$ (10)	Airmass <sup>j</sup> (11)	$S/N^{\text{k}}$ (12)
HE0507–3236	17.36	1.5770 (7)	1	–27.6	$\lesssim 0.51$	2003-10-22	J	180	18	1.23-1.09	25–20
HE0512–3329	17.03	1.5873 (7)	1	–28.0	$\lesssim 0.38$	2003-10-22	J	180	16	1.07-1.02	20–15
HE0926–0201	16.23	1.6824 (7)	1	–29.0	$\lesssim -0.33$	2004-02-11	J	180	12	1.11-1.17	30–10
HE0946–0500	16.24	1.1013 (7)	1	–28.0	$\lesssim 0.03$	2004-02-11	sZ	180	12	1.17-1.27	30
HE1003+0149	16.45	1.0809 (7)	1,2	–27.7	0.20	2004-02-13	sZ	180	12	1.19-1.14	20
HE1017–0009	16.69	1.1295 (7)	1	–27.6	0.87	2004-02-28	sZ	180	12	1.97-1.62	20–10
HE1104–1805	16.45	2.3192 (7)	1,2	–29.6	$\lesssim 0.19$	2004-02-11	sH	180	20	1.14-1.35	20
HE1249–0648	16.72	1.1940 (7)	1	–27.7	$\lesssim 0.23$	2004-02-05	sZ	180	16	1.04-1.06	30–15
HE1258–0823	16.26	1.1632 (7)	1	–28.1	$\lesssim 0.04$	2004-03-29	sZ	180	17	1.06-1.16	30

<sup>a</sup> Apparent B magnitude corrected because of Galactic absorption.

<sup>b</sup> Redshift, with uncertainty in parenthesis.

<sup>c</sup> Lines used for redshift calculations: 1: H $\beta$ , 2: [OIII] $\lambda$ 5007.

<sup>d</sup> Absolute B magnitude, computed for  $H_0=70 \text{ km s}^{-1}\text{Mpc}^{-1}$ ,  $\Omega_{\text{M}} = 0.3$ ,  $\Omega_{\Lambda} = 0.7$ , and  $k$ -correction spectral index  $a=0.6$ .

<sup>e</sup> Decimal logarithm of the specific flux ratio at 6cm and 4400 Å (effective wavelength of the B band). Upper limits are from the NVSS ( $\approx 2.5 \text{ mJy}$ ), and would place all undetected sources in the RQ domain.

<sup>f</sup> Date refers to time at start of exposure.

<sup>g</sup> Photometric band.

<sup>h</sup> Detector Integration Time (DIT) of ISAAC, in seconds.

<sup>i</sup> Number of exposures with single exposure time equal to DIT.

<sup>j</sup> Airmass at start and end of exposure.

<sup>k</sup>  $S/N$  at continuum level in the proximity of H $\beta$ . Two values are reported in case of different  $S/N$  on the blue and red side of H $\beta$  (blue side first). The  $S/N$  value is with N estimated at a  $2\sigma$  confidence level i.e., 2 times the rms.

**Table 2.** Measurements of Fluxes, Equivalent Widths and FWHM of Strongest Lines

Object name (1)	$F(\text{H}\beta_{\text{BC}})^{\text{a}}$ (2)	$W(\text{H}\beta_{\text{BC}})^{\text{b}}$ (3)	$W(\text{FeII}\lambda 4570)^{\text{c}}$ (4)	$\text{FWHM}(\text{FeII}\lambda 4570)^{\text{d}}$ (5)
HE0507–3236	$12.5 \pm 3.0$	$62 \pm 20$	$17 \pm 3$	$4100^{+1600}_{-900}$
HE0512–3329	$20.0^{+5.0}_{-3.0}$	$75^{+30}_{-10}$	$47 \pm 10$	$2400^{+1300}_{-500}$
HE0926–0201	$26.0 \pm 4.0$	$72 \pm 15$	$20 \pm 2$	$3400 \pm 1200$
HE0946–0500	$17.0^{+3.0}_{-2.0}$	$59^{+20}_{-10}$	$19^{+5}_{-3}$	$2900 \pm 1000$
HE1003+0149	$7.0 \pm 1.0$	$48 \pm 10$	$67 \pm 12$	$2100 \pm 1400$
HE1017–0009	$10.5 \pm 1.0$	$60^{+15}_{-10}$	$11^{+5}_{-3}$	$3600^{+2100}_{-1300}$
HE1104–1805	$20.0 \pm 4.0$	$72 \pm 15$	$39^{+7}_{-5}$	$4100 \pm 1700$
HE1249–0648	$15.5 \pm 2.0$	$63 \pm 15$	$31^{+5}_{-2}$	$1400^{+1000}_{-0}$
HE1258–0823	$24.0 \pm 3.0$	$44 \pm 10$	$20 \pm 4$	$1400^{+1000}_{-400}$

## Appendix B: Minimum $M_{\text{BH}}$ and $L/L_{\text{Edd}}$ as a Function of $z$

The absolute B magnitude  $M_{\text{B}}$  can be related to the specific luminosity at 5100 Å assuming an average spectral shape between 4400 (effective wavelength of B band) and 5100 Å. If the spectral shape is described by a power-law ( $f_{\nu} \propto \nu^{-b}$ ) with  $b = 0.3$  (Marziani et al., 2003b):

$$\log[\lambda L_{\lambda}(\lambda = 5100\text{\AA})] = -0.4M_{\text{B}} + 35.497. \quad (\text{B.1})$$

If we further assume that  $L = 10\lambda \cdot L_{\lambda}$ , with  $\lambda=5100$  Å i.e., a bolometric correction factor 10, we can write:

$$\log[\lambda L_{\lambda}(\lambda = 5100\text{\AA})] = \frac{L}{10 \cdot L_{\text{Edd}}} \cdot 1.3 \cdot 10^{47} M_{\text{BH},9\odot} \quad (\text{B.2})$$

where the black hole mass  $M_{\text{BH}}$  has been written in units of  $10^9 M_{\odot}$ . The absolute magnitude  $M_{\text{B}}$  is:

$$M_{\text{B}} = m_{\text{B}} + 5 - 5 \log d_{\text{L}} - 2.5(a-1) \log(1+z) \quad (\text{B.3})$$

where the luminosity distance  $d_{\text{L}}$  is in parsec, and the last term is the  $K(z)$  correction.

Assuming  $\Omega_{\text{M}} \neq 0$ ,  $\Omega_{\Lambda} \neq 0$ , and  $\Omega_{\text{k}} = 0$ , we have for the co-moving distance:

$$d_{\text{C}} = \frac{c}{H_0} \int_0^z \frac{dz'}{\sqrt{\Omega_{\text{M}}(1+z')^3 + \Omega_{\Lambda}}} \quad (\text{B.4})$$

This integral can be approximated with residuals less than 3% at all  $z$  (maximum error for  $z \rightarrow 0$ ).

$$d_{\text{C}} \approx \frac{c}{H_0} \left[ (1.500) (1 - e^{-\frac{z}{6.107}}) + 0.996 (1 - e^{-\frac{z}{1.266}}) \right] \quad (\text{B.5})$$

Object name (6)	F(H $\beta_{\text{NC}}$ ) <sup>e</sup> (7)	W(H $\beta_{\text{NC}}$ ) <sup>f</sup> (8)	W([OIII] $\lambda$ 4959) <sup>f</sup> (9)	W([OIII] $\lambda$ 5007) <sup>f</sup> (10)
HE0507–3236	7:	0.3:	2.7 $\pm$ 0.5	8.4 $\pm$ 0.6
HE0512–3329	3:	0.1:	2.5 $\pm$ 0.5	6.5 $\pm$ 1.0
HE0926–0201	28:	0.8:	5.6 $\pm$ 0.5	15.2 $\pm$ 1.0
HE0946–0500	14 $^{+9}_{-5}$	0.9	1.1 $\pm$ 0.5	3.4 $\pm$ 0.6
HE1003+0149	15 $^{+18}_{-5}$	1.0	0.6 $\pm$ 0.5	1.7 $\pm$ 0.5
HE1017–0009	15 $^{+10}_{-5}$	0.8	1.4 $\pm$ 0.5	3.8 $\pm$ 0.6
HE1104–1805	60 $\pm$ 18	2.0 $\pm$ 0.5	3.9 $\pm$ 0.5	11.4 $\pm$ 0.5
HE1249–0648	18 $\pm$ 5	0.7 $\pm$ 0.3	...	...
HE1258–0823	9:	0.8 $\pm$ 0.3	...	...

<sup>a</sup> Rest frame flux of H $\beta_{\text{BC}}$  in units of  $10^{-13}$  ergs s $^{-1}$  cm $^{-2}$  and  $\pm 2\sigma$  confidence level uncertainty.

<sup>b</sup> Rest frame equivalent width of H $\beta_{\text{BC}}$  in  $\text{\AA}$   $\pm 2\sigma$  confidence level uncertainty.

<sup>c</sup> Rest frame equivalent width of the FeII $\lambda$ 4570 blend in  $\text{\AA}$   $\pm 2\sigma$  confidence level uncertainty.

<sup>d</sup> FWHM of lines in the FeII $\lambda$ 4570 blend and uncertainty at  $2\sigma$ , in km s $^{-1}$ . See text for details.

<sup>e</sup> Rest frame flux of H $\beta_{\text{NC}}$  in units of  $10^{-16}$  ergs s $^{-1}$  cm $^{-2}$  and  $\pm 2\sigma$  confidence level uncertainty. Colons indicate highly uncertain values.

<sup>f</sup> Rest frame equivalent width of H $\beta_{\text{NC}}$ , [OIII] $\lambda$ 4959, and [OIII] $\lambda$ 5007 in  $\text{\AA}$ , with uncertainty at  $2\sigma$ . Colons indicate highly uncertain values.

**Table 3.** H $\beta_{\text{BC}}$  Line Profile Measurements

Source (1)	FWZI <sup>a</sup> (2)	$\Delta^{\text{a,b}}$ (3)	FWHM <sup>a</sup> (4)	$\Delta^{\text{a,b}}$ (5)	A.I. <sup>c</sup> (6)	$\Delta^{\text{b}}$ (7)	Kurt. <sup>d</sup> (8)	$\Delta^{\text{b}}$ (9)	c(0/4) (10)	$\Delta^{\text{a,b}}$ (11)
HE0507–3236	16000	2100	3500	300	−0.15	0.10	0.31	0.06	−500	1100
HE0512–3329	16000	3700	3100	300	−0.16	0.07	0.31	0.04	−100	1900
HE0926–0201	17000	1400	5100	500	0.21	$^{+0.07}_{-0.19}$	0.27	0.06	1200	700
HE0946–0500	20000	2800	3600	250	−0.06	0.09	0.37	0.05	−600	1400
HE1003+0149	9000	2100	2900	280	−0.06	$^{+0.07}_{-0.11}$	0.33	0.05	−400	1000
HE1017–0009	16000	3800	6200	290	−0.04	$^{+0.08}_{-0.05}$	0.41	0.04	200	1900
HE1104–1805	15000	1500	4300	260	0.11	0.09	0.38	0.05	900	800
HE1249–0648	21000	1000	4900	500	0.13	$^{+0.11}_{-0.07}$	0.31	0.05	1400	500
HE1258–0823	17000	2600	4400	500	−0.08	$^{+0.20}_{-0.08}$	0.23	0.06	−700	1300

The luminosity distance is:

$$d_L = d_C(1 + z) \quad (\text{B.6})$$

and we can use the new relationship to derive a working relationship for  $M_{\text{BH}}$ :

$$M_{\text{BH},9\odot} = 3.85 \cdot 10^6 h^{-2} \left( \frac{L}{L_{\text{Edd}}} \right)^{-1} \cdot 10^{-0.4m_B} \cdot [1.5(1 - e^{-\frac{z}{6.107}}) + (1 - e^{-\frac{z}{1.266}})]^2 (1 + z)^{(1-a)}$$

where  $h = H_0/75$ . Curves shown in Figs. 3, 5, 6, 7 assume  $a = 0.6$ . Differences for  $0.3 \lesssim a \lesssim 0.6$  are minor.

## References

- Aoki, K., Kawaguchi, T., & Ohta, K. 2005, ApJ, 618, 601  
 Bachev, R., Marziani, P., Sulentic J. W., Dultzin-Hacyan D., Calvani M., ApJ, in press  
 Baldwin, J. A., et al. 1996, ApJ, 461, 664  
 Bernardi, M., et al. 2003, AJ, 125, 1866  
 Bernardi, M., et al. 2005, ArXiv Astrophysics e-prints, arXiv:astro-ph/0510696  
 Boroson, T. A. 2003, ApJ, 585, 647  
 Boroson, T. 2005, ArXiv Astrophysics e-prints, arXiv:astro-ph/0505127  
 Boroson, T. A., & Green, R. F. 1992, ApJS, 80, 109  
 Boyle, B. J., Shanks, T., Croom, S. M., Smith, R. J., Miller, L., Loaring, N., & Heymans, C. 2000, MNRAS, 317, 1014  
 Brotherton, M. S., Wills, B. J., Steidel, C. C., & Sargent, W. L. W. 1994, ApJ, 423, 131  
 Brotherton, M. S. 1996, ApJS, 102, 1  
 Collin-Souffrin, S., Dyson, J. E., McDowell, J. C., & Perry, J. J. 1988, MNRAS, 232, 539

Source (12)	c(1/4) (13)	$\Delta^{a,b}$ (14)	c(1/2) <sup>a</sup> (15)	$\Delta^{a,b}$ (16)	c(3/4) <sup>a</sup> (17)	$\Delta^{a,b}$ (18)	c(0.9) <sup>a</sup> (19)	$\Delta^{a,b}$ (20)
HE0507–3236	–300	300	50	150	100	90	90	50
HE0512–3329	–500	200	–180	150	–80	80	–30	50
HE0926–0201	800	<sup>+400</sup> <sub>–1100</sub>	–150	250	–160	130	–110	80
HE0946–0500	–300	200	–320	120	–160	100	–70	70
HE1003+0149	–100	200	–50	130	–20	70	10	50
HE1017–0009	–900	300	–610	130	–350	140	–360	120
HE1104–1805	200	300	–180	130	–190	120	–190	80
HE1249–0648	400	400	–70	240	–60	130	–110	80
HE1258–0823	–400	<sup>+700</sup> <sub>–300</sub>	–330	220	–30	110	–40	50

<sup>a</sup> In units of km s<sup>–1</sup>.

<sup>b</sup> 2 $\sigma$  confidence level uncertainty.

<sup>c</sup> Asymmetry index defined as in Marziani et al. (1996).

<sup>d</sup> Kurtosis parameter as in Marziani et al. (1996).

- Corbin, M. R. 1991, *ApJ*, 375, 503
- Corbin, M. R., & Francis, P. J. 1994, *AJ*, 108, 2016
- de Robertis, M. 1985, *ApJ*, 289, 67
- Ferrarese, L., & Merritt, D. 2000, *ApJL*, 539, L9
- Gaskell, C. M. 1982, *ApJ*, 263, 79
- Gebhardt, K., et al. 2000, *ApJL*, 539, L13
- Giveon, U. et al. 1999, *MNRAS*, 306, 637
- Gregg, M. D., Wisotzki, L., Becker, R. H., Maza, J., Schechter, P. L., White, R. L., Brotherton, M. S., & Winn, J. N. 2000, *AJ*, 119, 2535
- Grupe, D., Beuermann, K., Mannheim, K., & Thomas, H.-C. 1999, *A&A*, 350, 805
- Jackson, N., Perez, E., & Penston, M. V. 1991, *MNRAS*, 249, 577
- Joly, M. 1988, *AAp*, 192, 87
- Kaspi S., Smith P.S., Netzer H., et al. 2000, *ApJ*, 533, 631
- Kaspi, S., Maoz, D., Netzer, H., Peterson, B. M., Vestergaard, M., & Jannuzi, B. T. 2005, *ArXiv Astrophysics e-prints*, arXiv:astro-ph/0504484
- Koratkar, A. P., & Gaskell, C. M. 1991, *ApJL*, 370, L61
- Krolik, J. H. 2001, *ApJ*, 551, 72
- Kuraszkiewicz, J. K., Green, P. J., Crenshaw, D. M., Dunn, J., Forster, K., Vestergaard, M., & Aldcroft, T. L. 2004, *ApJS*, 150, 165
- Laor, A. 2001, *ApJ*, 553, 677
- Malkan, M. A., & Sargent, W. L. W. 1982, *ApJ*, 254, 22
- Marconi, A., & Hunt, L. K. 2003, *ApJ*, 589, L21
- Marziani, P., & Sulentic, J. W. 1993, *ApJ*, 409, 612
- Marziani P., Sulentic J.W., Dultzin-Hacyan D., Calvani M., Moles M., 1996, *ApJS* 104, 37
- Marziani P., Sulentic J.W., Zwitter T., Dultzin-Hacyan D., Calvani M., 2001, *ApJ*, 558, 553 (M01)
- Marziani P., Sulentic J. W., Zamanov R., Calvani M., Dultzin-Hacyan D., Bachev R., Zwitter T., 2003a, *ApJS*, 145, 199 (M03)
- Marziani, P., Zamanov, R., Sulentic, J. W., Dultzin-Hacyan, D., Bongardo, C., & Calvani, M. 2003b, *ASP Conf. Ser. 290: Active Galactic Nuclei: From Central Engine to Host Galaxy*, 229
- Marziani P., Zamanov R., Sulentic J. W., Calvani M., 2003c, *MNRAS*, 345, 1133 S. 2000, *MNRAS*, 314, L17
- Mathur, S., Kuraszkiewicz, J., & Czerny, B. 2001, *New Astronomy*, 6, 321
- McIntosh, D. H., Rieke, M. J., Rix, H.-W., Foltz, C. B., & Weymann, R. J. 1999, *ApJ*, 514, 40
- McLure, R. J., & Dunlop, J. S. 2001, *MNRAS*, 327, 199
- McLure, R. J., & Dunlop, J. S. 2004, *MNRAS*, 352, 1390
- McLure, R. J., & Jarvis, M. J. 2004, *MNRAS*, 353, L45
- McLure, R. J., Jarvis, M. J., Targett, T. A., Dunlop, J. S., & Best, P. N. 2005, *ArXiv Astrophysics e-prints*, arXiv:astro-ph/0510121
- Metcalfe, R. B., & Magliocchetti, M. 2006, *MNRAS*, 365, 101
- Netzer, H. 2003, *ApJ*, 583, L5
- Onken, C. A., Ferrarese, L., Merritt, D., Peterson, B. M., Pogge, R. W., Vestergaard, M., & Wandel, A. 2004, *ApJ*, 615, 645
- Osterbrock, D. E., & Shuder, J. M. 1982, *ApJS*, 49, 149
- Peng, C. Y., Impey, C. D., Ho, L. C., Barton, E. J., & Rix, H.-W. 2005, *ArXiv Astrophysics e-prints*, arXiv:astro-ph/0509155
- Peterson, B. M., & Wandel, A. 1999, *ApJL*, 521, L95
- Peterson, B. M., & Wandel, A. 2000, *ApJ*, 540, L13
- Peterson, B. M., et al. 2004, *ApJ*, 613, 682
- Reimers, D., Koehler, T., & Wisotzki, L. 1996, *AApS*, 115, 235
- Richards, G. T., Vanden Berk, D. E., Reichard, T. A., Hall, P. B., Schneider, D. P., SubbaRao, M., Thakar, A. R., & York, D. G. 2002, *AJ*, 124, 1
- Rokaki, E., Lawrence, A., Economou, F., & Mastichiadis, A. 2003, *MNRAS*, 340, 1298
- Shang, Z., et al. 2004, *ArXiv Astrophysics e-prints*, astro-ph/0409697
- Sheth, R. K., et al. 2003, *ApJ*, 594, 225
- Shemmer, O., Netzer, H., Maiolino, R., Oliva, E., Croom, S., Corbett, E., & di Fabrizio, L. 2004, *ApJ*, 614, 547
- Shields, J. C., Ferland, G. J., & Peterson, B. M. 1995, *ApJ*, 441, 507

- Stirpe, G. M. 1990, A&AS, 85, 1049
- Sulentic, J. W. 1989, ApJ, 343, 54
- Sulentic, J. W., Zheng, W., Calvani, M., & Marziani, P. 1990, ApJ, 355, L15
- Sulentic, J. W., Marziani, P., & Dultzin-Hacyan, D. 2000a, ARA&A, 38, 521
- Sulentic, J. W., Marziani, P., Zwitter, T., Dultzin-Hacyan, D., & Calvani, M. 2000b, ApJ, 536, L5
- Sulentic, J. W., Marziani, P., Zwitter, T., Dultzin-Hacyan, D., & Calvani, M. 2000c, ApJL, 545, L15
- Sulentic, J. W., Marziani, P., Zamanov, R., Bachev, R., Calvani, M., & Dultzin-Hacyan, D. 2002, ApJ, 566, L71
- Sulentic J. W., Zamfir S., Marziani P., Bachev R., Calvani M., Dultzin-Hacyan D., 2003, ApJ, 597, L17
- Sulentic, J. W., Stirpe, G. M., Marziani, P., Zamanov, R., Calvani, M., & Braito, V. 2004, AAp, 423, 121 (Paper I)
- Sulentic, J. W., Dultzin-Hacyan, D., Marziani, P., Bongardo, C., Braito V., Zamanov, R., Calvani, M. 2006, RevMexAAp, accepted
- Treu, T., Malkan, M. A., & Blandford, R. D. 2004, ApJ, 615, L97
- Véron-Cetty, M.-P., Véron, P., & Gonçalves, A. C. 2001, A&A, 372, 730
- Vestergaard, M. 2002, ApJ, 571, 733
- Vestergaard, M., & Peterson, B. M. 2005, ApJ, 625, 688
- Vestergaard, M., & Peterson, B. M. 2006, astro-ph/0601303
- Wandel, A., Peterson, B. M., & Malkan, M. A. 1999, ApJ, 526, 579
- Wanders, I., et al. 1995, ApJL, 453, L87
- Wang, J. 2003, AJ, 125, 2859
- Wang, J., Wei, J. Y., & He, X. T. 2005, A&A, 436, 417
- Wills, B. J., Netzer, H., & Wills, D. 1985, ApJ, 288, 94
- Wisotzki, L., Koehler, T., Ikonomidou, M., & Reimers, D. 1995, A&A, 297, L59
- Wisotzki, L., Koehler, T., Kayser, R., & Reimers, D. 1993, A&A, 278, L15
- Wisotzki, L., Christlieb, N., Bade, N., Beckmann, V., Köhler, T., Vanelle, C., & Reimers, D. 2000, A&A, 358, 77
- Wu, X.-B., Wang, R., Kong, M. Z., Liu, F. K., & Han, J. L. 2004, AAp, 424, 793
- Wucknitz, O., Wisotzki, L., Lopez, S., & Gregg, M. D. 2003, A&A, 405, 445
- Zamanov, R., Marziani, P., Sulentic, J. W., Calvani, M., Dultzin-Hacyan, D., & Bachev, R. 2002, ApJ, 576, L9

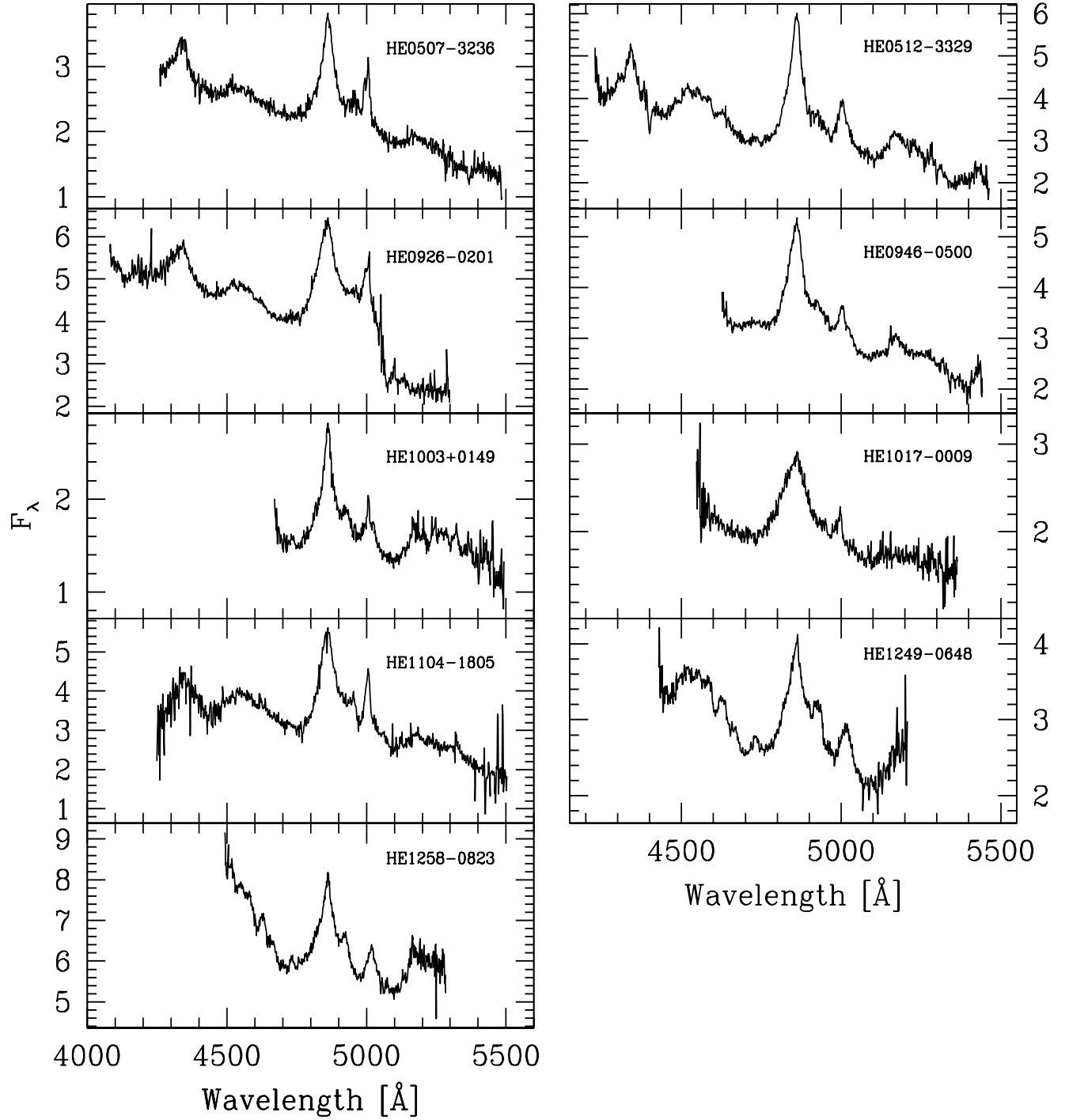


**Fig. 1.** Calibrated VLT-ISAAC spectra for 9 new intermediate-redshift quasars. Abscissæ are rest-frame wavelength in  $\text{\AA}$ , ordinates the rest-frame specific flux in units of  $10^{-15} \text{ ergs s}^{-1} \text{ cm}^{-1} \text{ \AA}^{-1}$ .

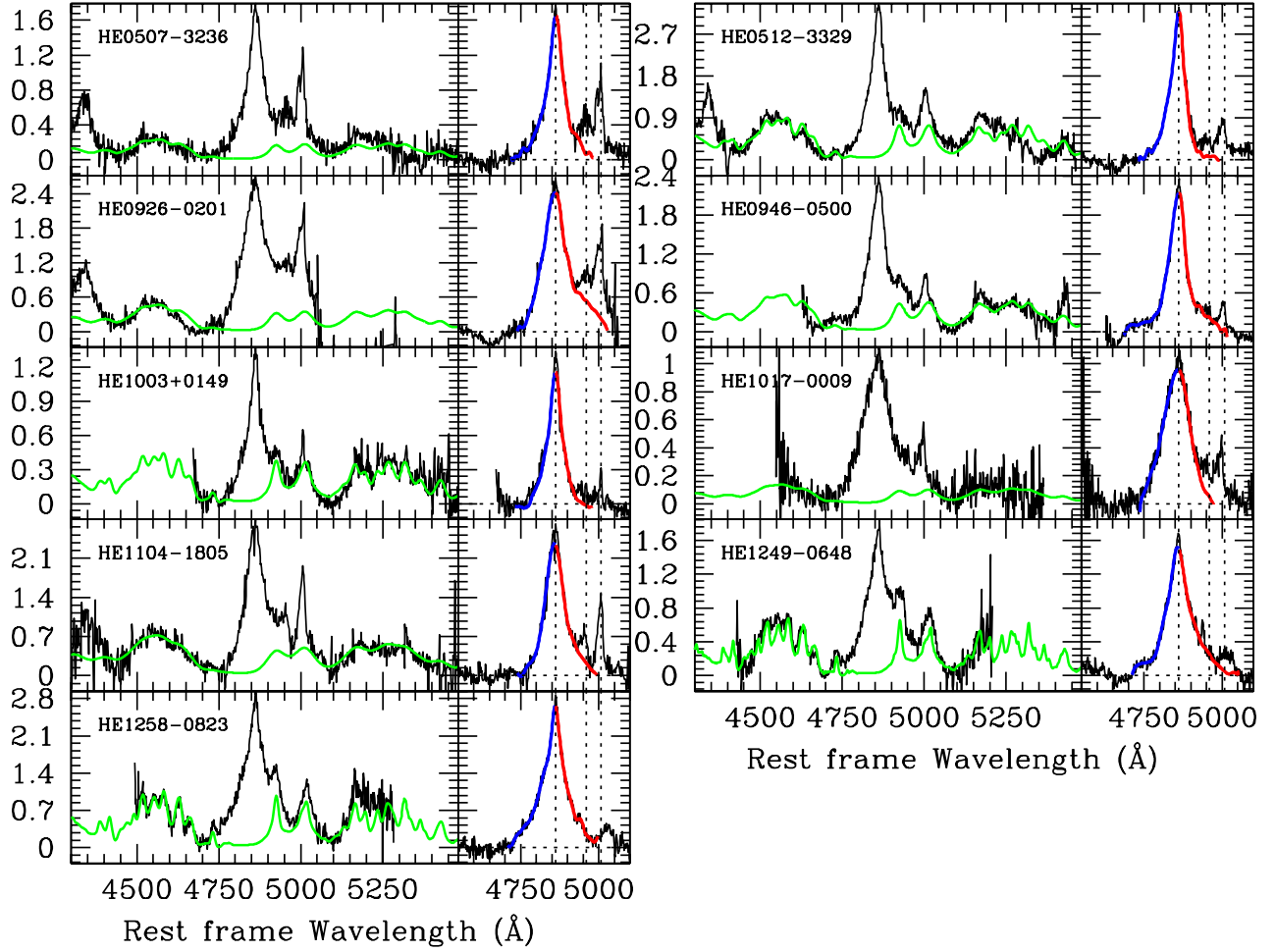


**Fig. 2.** Spectral Atlas for the new intermediate-redshift quasars. Left-hand panels show the continuum-subtracted  $H\beta$  spectral region. Axes are the same as Fig. 1. The best-fit Fe II emission model is traced as a thin (green) line. Right-hand panels show the enlarged  $H\beta$  profiles after continuum and Fe II subtraction. The (blue and red) thick line shows a spline fit of the short and long wavelength sides of the  $H\beta_{\text{BC}}$  profile, respectively.



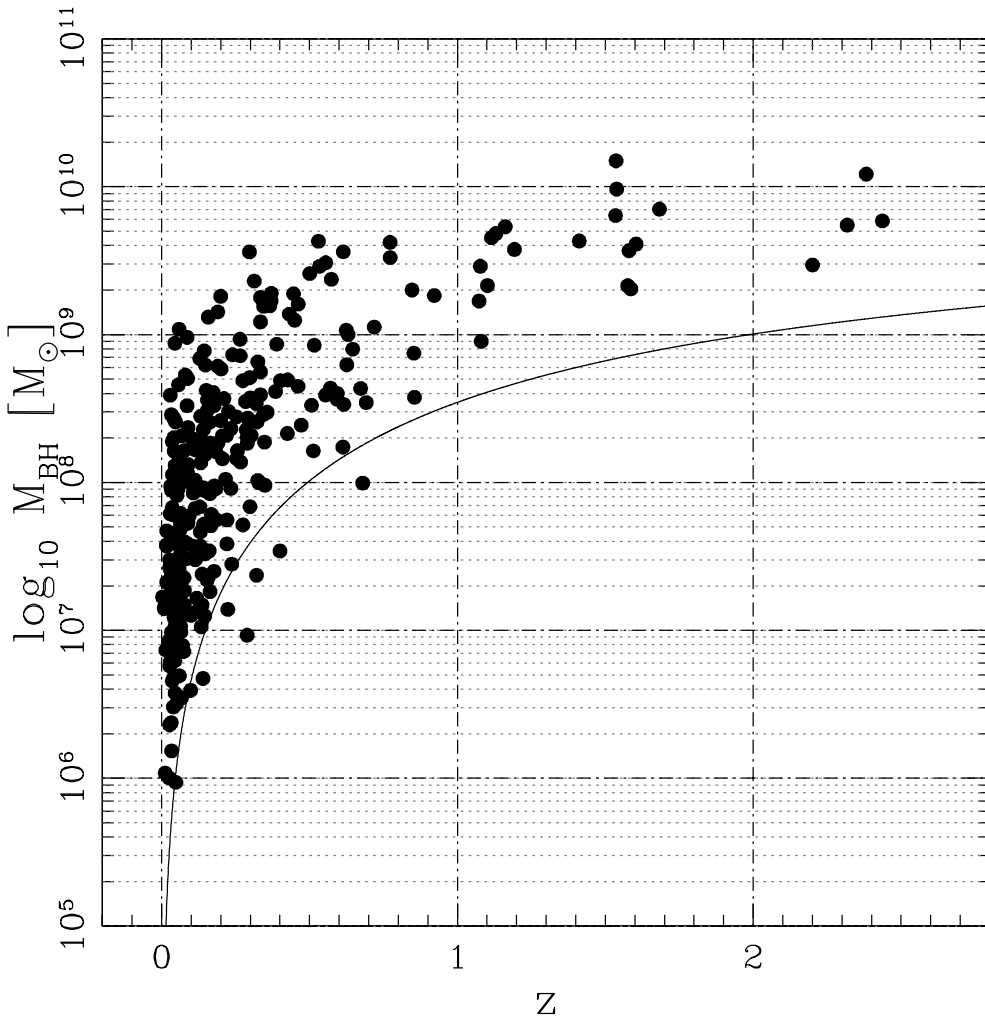


**Fig. 3.** Distribution of  $M_{\text{BH}}$  estimates as a function of  $z$  using uncorrected  $\text{FWHM}(\text{H}\beta_{\text{BC}})$  values. Intermediate  $z$  sources observed with ISAAC are at  $z \gtrsim 0.8$ . The solid curve estimates the minimum detectable  $M_{\text{BH}}$  for our sample – see text.

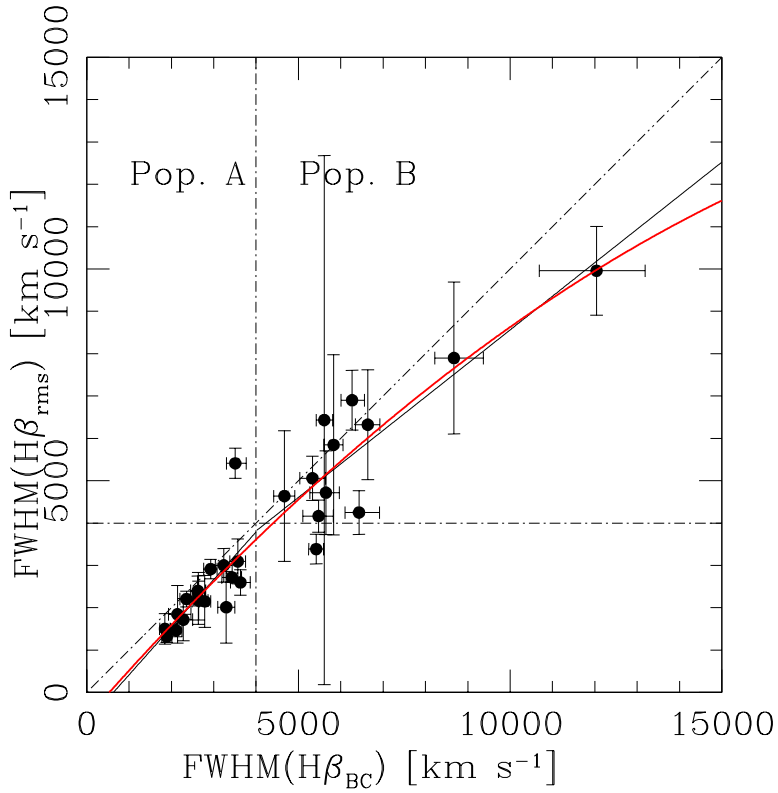


**Fig. 4.** FWHM measured from the variable part of the  $\text{H}\beta_{\text{BC}}$  profile for low- $z$  sources with reverberation data (Peterson et al., 2004) versus  $\text{FWHM}(\text{H}\beta_{\text{BC}})$  ( $\text{km s}^{-1}$ ) measures from Marziani et al. (2003c). Solid straight lines show best fits for  $\text{FWHM}(\text{H}\beta_{\text{BC}}) \leq 4000 \text{ km s}^{-1}$  (Pop. A) and for sources with broader lines (Pop. B). The solid curve shows a weighted least-square fit of all data with a second order polynomial. The diagonal dot-dashed line indicates the location of equal ordinate and abscissa values.

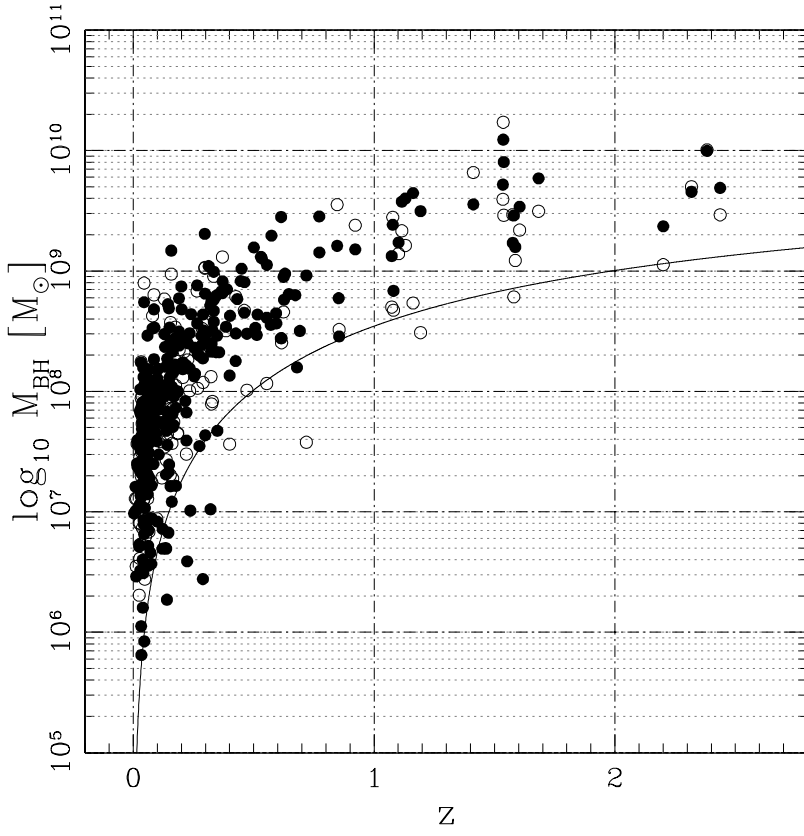


**Fig. 5.**  $M_{\text{BH}}$  computed from corrected  $\text{FWHM}^{\text{corr}}(H\beta_{\text{BC}})$  as a function of  $z$  (filled circles).  $M_{\text{BH}}$  estimates computed from  $\text{FWHM}(\text{FeII}\lambda 4570)$  measures are shown as open symbols. Symbol types and solid curve are as described for Fig. 3.

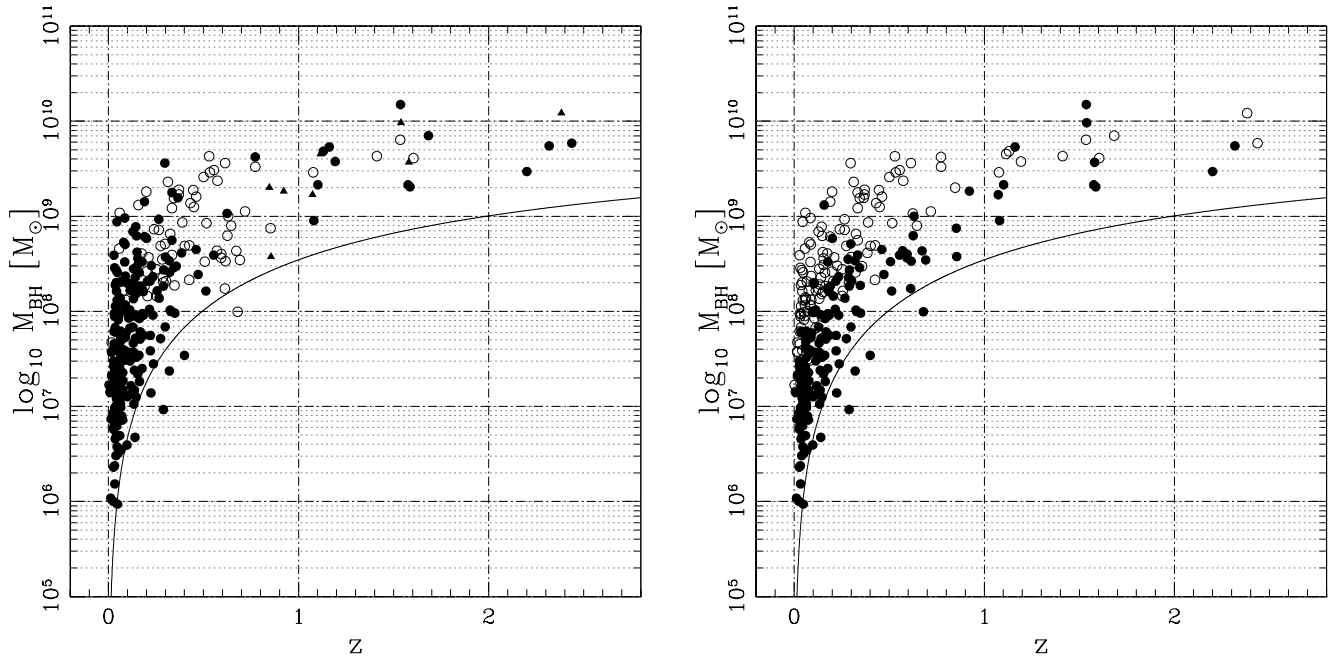


**Fig. 6.**  $M_{\text{BH}}$  computations using same samples as Fig. 3, where RQ and RL sources are indicated by filled and open symbols respectively (upper panel). Triangles indicate sources for which radio data are insufficient to compute a meaningful  $R_K$ . The lower panel distinguishes  $M_{\text{BH}}$  for Pop. A (filled symbols) and Pop. B (open symbols). The solid curve is as described for Fig. 3.

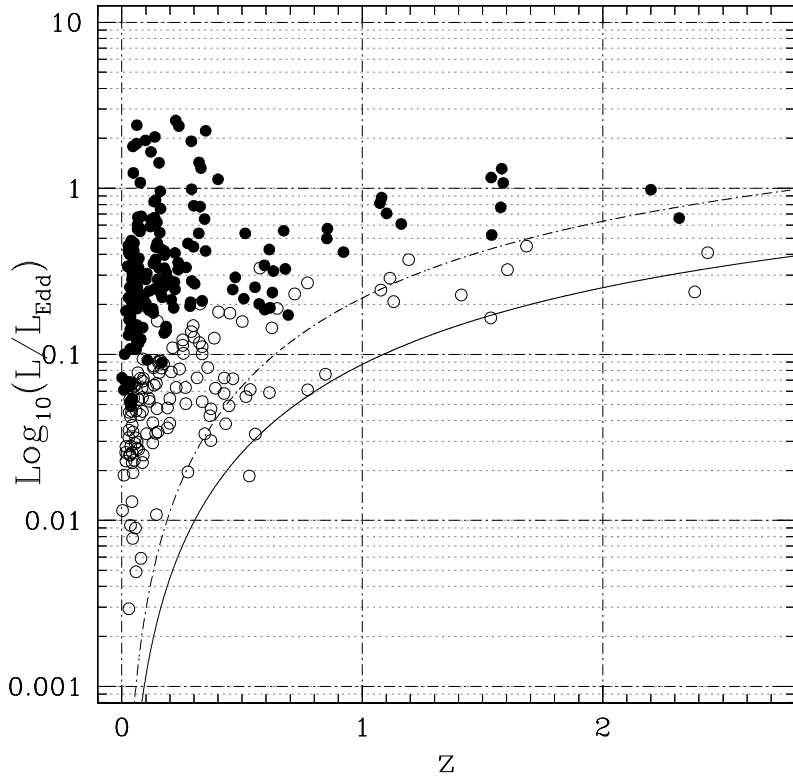


**Fig. 7.** Distribution of  $L/L_{\text{Edd}}$  with  $z$  following Fig. 3 with  $\lambda L_\lambda$  values derived from the  $5100 \text{ \AA}$  rest-frame flux and with  $\alpha = 0.67$ . E1 Populations A and B are indicated by filled and open symbols respectively. The solid line traces the minimum  $L/L_{\text{Edd}}$  for a fixed mass value of  $4 \cdot 10^9 M_\odot$  to observe a quasar above the limiting magnitude of the HE quasar survey  $m_B \approx 17.5$ . The dot-dashed lines indicate the same limit but assuming limiting magnitude  $m_B \approx 16.5$ .